The University of Manchester Institute of Science and Technology

CHARACTERISATION OF NATURAL AEROSOL IN W. EUROPE AND INVESTIGATION OF DEPOSITION TO IRREGULAR TOPOGRAPHY

FINAL REPORT - JULY 1988

to

US ARMY - DAJA45-87-C-0017

2

CHARACTERISATION OF NATURAL AEROSOL IN W. EUROPE AND INVESTIGATION OF DEPOSITION TO IRREGULAR TOPOGRAPHY

FINAL REPORT - JULY 1988

to
US ARMY - DAJA45-87-C-0017

by

T W Choularton, M W Gallagher and K Beswick

Department of Pure and Applied Physics

UMIST
P O Box 88
Manchester M60 1QD

INTRODUCTION

In this report we present the work performed under this contract not described in the two progress reports already submitted. The object of the work was to invesyigate factors afecting the natural fate of aerosol and chemical agents during transport in Western Europe. We have investigated rainout occult and dry deposition.

In section 2 of the report we describe measurements of the turbulent deposition of cloud droplets (size>1μm) and dissolved chemical agents to a grass covered hill side. In section 3 these results are used to predict the deposition of chemical agents to elevated topography of a wide range of scales. These are compared with deposition rates associated with rain-out using a model of the seeder-feeder effect.

In section 4 we describe results of an experiment to measure the turbulent deposition of sub-micron aerosol by eddy correlation. In section 5 we present the results of the UMIST contribution to a joint aerosol transport experiment conducted by UMIST and the University of Galway. In section 6 the main conclusions of the work are summarised.

Section 2

Report on the Measurements of the Size Dependence of Cloud Droplet Deposition at a Hill Site.

Abstract

Measurements have been made of the deposition of cloud droplets and dissolved chemical species to a grass moorland vegetation. Measurements of liquid water fluxes have been made by the gradient technique using Knollenberg FSS probes and by a weighing lysimeter. Deposition velocities for cloud liquid water in the range 0.1 to 0.24 g m^{-3} at 1.0 m were close to those for momentum. The FSS probes enabled the determination of deposition velocities as a function of droplet size. It was found that the deposition velocity increased with droplet radius from 2.5 μm to 6.5 μm radius. Between 6.5 and 12.5 μm radius deposition velocities exceeded those for momentum but decreased sharply between 12.5 and 15.5 μm.

In periods of thin cloud (<0.1 g m^{-3}) evaporation from the surface occurred despite continued deposition.

1 Introduction

It has been known for some time that the direct deposition of droplets, so-called 'occult deposition', (Nagel 1956; Kerfoot 1968), may be an important pathway for the deposition of pollutants. Relatively few measurements have been made. Dollard and Unsworth (1983) used May impactors to measure gradients in liquid water content from which deposition velocities were calculated. Similar measurements were performed by Dollard et al. (1983) where some preliminary measurements of ion fluxes associated with the liquid water fluxes were made. In this paper we present detailed measurements of droplet flux, and the associated chemical deposition, by two different techniques and investigate the variation of deposition velocity with droplet size.

A large collaborative experiment is in progress at Great Dun Fell in Cumbria, UK, 847 m. asl, to investigate aqueous phase cloud chemical processes and deposition of species in aqueous solution to the hill surface. Results from the cloud chemistry experiments have been described by Chandler *et al.* (1988) and results from measurements of the altitudinal variation of wet deposition by rainfall in Choularton *et al.* (1988) and Fowler *et al.* (1988). Full details of the area and the measurements made at each site may be found in these papers.

In this paper we describe measurements of the deposition of cloud droplets to the moorland vegetation on the hillside. This was done both by using the gradient technique and measuring the rate of increase in weight of a representative section of turf placed on a lysimeter. Simultaneous measurements of the chemical composition of the cloud water were made enabling fluxes of the major species to the surface to be deduced. The measurements were made on the S.W. face of Great Dun Fell about 150 m below the hill summit which rises 650 m above the Eden Valley to the S.W. This area is uniformly covered by rough grass and measurements made at this site using Porton anemometers have shown a very good logarithmic wind profile in the lowest 3 m of the boundary layer in conditions of cloud and strong winds. These measurements indicate that the site is well suited to the use of the gradient technique. Further details of the airflow and turbulence characteristics may be found in Gallagher *et al.* (1988).

2 Theory

Cloud droplets are transported to the surface by eddy diffusion and gravitational sedimentation. The droplet flux, F, within the surface layer is given by e.g. Chamberlain (1967) and can be written

$$F = K(z)\frac{\partial C}{\partial z}(z,r) + V_S(r)\,C(z,r) = V_d(z,r)\,C(z,r) \qquad (1)$$

where C (z,r) is the concentration at height z for a given size, K (z) is the vertical eddy diffusivity, V_S (r) the terminal velocity of the droplet and V_d (z,r) the deposition velocity. Since the flux near the surface is a constant and assuming neutral stability, K (z) = kzu_*, k is Von Karmans constant, then the solution to (1) becomes

$$V_d(z,r) = \frac{V_S(r)}{\{\,1 - (z/z_0)^{-V_s(r)\,/\,ku_*}\,\}} \qquad (2)$$

for which it is assumed that $C(z=z_0)$, where z_0 is the roughness length. This result has been used to model the deposition of chemical species in cloud droplets to hill surfaces by Hill *et al.* (1987).

If droplet capture at the surface is not rate limiting and if $u_* \gg V_S$ (r), then the concentration profile is independent of droplet size, and the usual logarithmic profile is obtained for C. The deposition velocity in this case is then the deposition velocity due to momentum only viz, V_m (z) $\approx ku_*/\ln(z-d)$. By measuring $\partial C(z,r)/\partial z$ and $\underline{K}(z)$ we obtain V_d (z,r) using (1).

3 Experimental Procedure.

Figure 1 shows the experimental arrangement used. A 4 m scaffolding tower was erected on the hill side , at an elevation of 575 m above the valley floor. This site has been described in detail by Fowler *et al.* (1988) and is essentially an elevated moorland site dominated by tussocks of *Eriophorum sp* and *Juncus sp* and providing extensive homogeneous fetches, greater than 300 m, in most directions. Two independent methods were employed to measure the cloud droplet deposition process, a gradient technique and a direct weighing lysimeter method.

4 Gradient Method.

Two Knollenberg forward scattering spectrometer probes, FSSP, were mounted on the tower, at 0.5 m and 3.5 m above the surface. These probes were set to size cloud droplets in the range 1 to 15 μm radius with a resolution of 0.5 μm radius. Since mean droplet sizes at this site are typically 5 to 7 μm radius this setting is ideally suited for measurements of liquid water content obtained by integrating resulting number spectra. Both probes were aspirated at 26.5 ms^{-1} using Rotron ducted fans. Variations in sample volume which result from wind ramming and gusting were corrected for using the techniques described in detail by Choularton *et al* (1986).

One of the probes had previously been compared with several different liquid water content measuring techniques. These included a Barnes infrared transmissometer operating on 10.6 μm wavelength, Consterdine (1984) and a laser scattering device Latham *et al* (1984). The agreement by these independent methods was good with mean errors of ± 10 %, and extrema of ± 20 %. Thus the error in absolute liquid water content using these devices is at worst ± 10 %.

In adopting the gradient technique, the second probe was normalized to the 'calibrated' probe. This was done by running both probes side by side at 0.5 m above the surface in conditions with liquid water contents in the range 0.2 to 0.5 gm m^{-3}. Commercial nebulizers were also used for intercomparison purposes . The probes were sampled at 1 Hz and integrated over typically 15 to 30 minutes to reduce the sampling errors in the larger size ranges of 12.5-15.5 μm where number concentrations were low. This enabled channel by channel normalization factors to be obtained. The standard errors in these factors were at most 4 % for sizes up to 10 μm and 15 % for sizes up to 15.5 μm. Under low liquid water content regimes (< 0.1 g m^{-3}) these errors increased significantly. The intercomparison between the two probes is discussed in detail later.

The large separation of the probes meant that observed gradients would be substantially greater than the corresponding error in the gradient measurements except in the case of the largest droplets. Thus detailed measurements of gradients in number concentration as a function of drop size could be obtained with confidence. The disadvantage with this large separation , however, is that a larger uninterrupted fetch is required with additional increases in advection errors occurring. A large number of

measurements at this site have confirmed, however, that the wind profile is closely logarithmic up to the level of the higher probe.

5 Direct Weighing Method.

A direct weighing lysimeter was installed next to the scaffold tower as shown in Figure 1. The instrument and the logging system has been described in detail by Calder *et al.* (1984). Essentially the system consisted of a Sartorius 3806MP electronic balance with a 1.0 gm accuracy in 30 kg. The balance was placed in a hole 1.5 m deep. A plastic weighing tray was then placed on top of this flush with the surface of the ground. The turf which had been removed prior to digging the hole was replaced in the tray. The collecting area of the tray was 0.64 m^2. Polystyrene sections were mounted between the balance and the tray to exclude any heat transfer from the balance mechanism to the tray producing unwanted evaporation effects. The balance was interrogated by a microcomputer, with a sampling rate of 1 Hz . This data was then averaged to 1 minute before being written to magnetic disc.

6 Additional Measurements.

Measurements of U_* were obtained from a set of precision Porton cup anemometers mounted on a 3 m tower. The anemometers had previously been calibrated in a wind tunnel. Additional wind speed measurements were made at 3 m and 10 m using standard Vector Instruments cup anemometers. The output from the profile anemometers was integrated over 15 minute periods.

The data from the two FSSP's, 3 and 10 m wind speeds and directions, temperature at 2 m, and a variety of air and cloud water chemical parameters e.g. pH, aqueous phase H_2O_2, gas phase SO_2 and gas phase O_3 were logged continuously at 1 Hz as described by Choularton *et al.* (1988). In addition bulk samples of cloud water were collected on an event basis for later analysis by ion-chromatography.

7 Intercomparison of FSS Probes and Treatment of Data.

To obtain high quality data in an experiment of this kind precautions have to be taken with FSS probes. Unless the optical alignment of these probes is carefully checked systematic differences between individual probes will

occur. In order to obtain accurate relative differences between two probes sampling different regions of a cloud which have undergone different levels of depletion near the ground, consistent normalisation factors must be obtained. For measurements of total liquid water content where the bulk of the liquid water is contained within a narrow spectrum of drop sizes the criteria for accurate normalisation factors will not be as rigorous as for comparison of individual size classes. The accuracy of these correction factors will necessarily determine the accuracy with which the concentration gradient can be measured as a function of droplet size.

Care must be taken to assess the various errors involved in channel by channel comparison. These are

1) Sample error of the FSSP.
2) Wind ramming and gust effects on the sample volume at different levels, and
3) Errors in the normalisation factors.

The sample error can be reduced by using sufficiently long averaging times. Figure 2 shows a typical cloud droplet spectrum observed at this site by Probe 2, mounted at 3.5 m. The data were averaged over 15 minutes. The liquid water content,L, was 0.24 g m^{-3} , the number concentration N = 180 cm^{-3}, and the mean radius R = 5.9 µm. The sample errors for this run are of the order 0.3 % rising to 2.7 % for the largerst drops. Because of the depletion in liquid water content the lower probe produced sample errors of the order of 2.1 % rising to 15.7 % for the largest drops when the normalisation factors are taken into account. For periods where the liquid water content was small (< 0.1 g m^{-3}) the errors for the large drops became excessively large (>50 %). Such periods were characterised by variable cloud base with large scale inhomogeneities in the sampled cloud. In extreme cases this inhomogeneity could be observed on scales less than the probe separation. Data from such periods has been excluded from the analysis presented here.

The error due to wind ramming is corrected for through the use of the following relation ;

$$S_a = S_0 \left(1 + \frac{u}{u_a} \right) \qquad (3)$$

where S_a is the actual sample volume, S_0 is the sample volume under zero wind conditions, u is the local wind speed measured at the probe level,

8

and u_a is the aspiration speed of the fan which is 26.5 m s^{-1}. Provided the probes are oriented into wind and the wind speed at each level is known to a reasonable degree of accuracy (derived from the profile data) then the sample volume error should be small. The sample volume correction can also be made using the droplet transit time method described by Choularton *et al* (1986). Agreement between the two methods for Probe 2 was good agreeing to within 15 %.

Figure 3 shows the results obtained from seven 10 minute intercomparison runs prior to the experiment where the probes were run side by side. R is the mean of the ratios of the concentrations for Probe 1 to Probe 2 as a function of radius. The vertical bars represent the standard errors for each FSS probe bin size. These were of the order of 2 % for drops up to 10 μm and rose to typically 15 % for 15μm drops. When the probes are separated vertically the data from each channel of probe 1 is multiplied by the appropriate normalisation factor. The liquid water gradient, or the gradient in the number concentration, in each channel between the two heights can be calculated. The errors being generated by combining the sample errors from the two probes and the error in R

3 Experimental Results

Table 1 shows details of several runs obtained during the early hours of the morning of 11th June 1987 over a three hour period. The wind during this period was approximately 10 ms^{-1}, from 030^0. Temperatures, measured at 2.0 m, varied from 3.8 to 4.0 ^{0} C. Figure 4 is a trace of liquid water content calculated from the droplet histograms recorded by the FSSP mounted at 3.5 m for the period 00:00 to 12:00 hrs G.M.T. The large variation in cloud base is evident. Mean liquid water contents varied from near zero to 240 mgm^{-3}. Values of u_*, z_o and d were obtained from the Porton anemometer tower. In each case very good logarithmic profiles were obtained as shown e.g. in Figure 5. Unfortunately during the experiment two of the profile anemometers ceased to operate and information was only available from four levels. A large number of similar measurements at this site with the full complement of anemometers show excellent logarithmic profiles consistent with the measurements presented here. Table 2 contains the bulk deposition parameters calculated for each run. It was found that for periods of low liquid water content e.g Runs 2 and 8 it became difficult to determine a reliable profile of concentration due to very large short term fluctuations

in liquid water content. This is reflected by the ratios of v_t to v_m which are much greater than 1. If these two runs are ignored then the mean ratio $v_t/v_m = 0.96 \pm 0.12$.

Figure 6 shows the measurements obtained from the lysimeter for the period 00:34 to 02:00. Frequent calibration of the instrument was made, particularly when the site went out of cloud. During this initial period the increasing trend due to water transfer from the cloud to the balance is clear, however, the noise on the trace due to the variability in the cloud meant that the error on the mean slope was large for individual runs, as is indicated in Table 3, where because of evaporation a negative trend could be observed in some cases. The errors shown for the lysimeter are the standard errors of the slope.

Better agreement could be obtained for periods of cloud where conditions were relatively steady e.g. combining runs 3 & 4 gave a lysimeter flux of 11 $\pm$ 3 mg m^{-2} s^{-1} compared to a cloud droplet flux of 8.8 $\pm$ 1.1 mg m^{-2} s^{-1}. This corresponded to a period of substantial liquid water content which remained reasonably constant so that little evaporation from the surface of the lysimeter occurred. During this period no precipitation was reported. Even very light drizzle will dominate the water flux to the lysimeter but will not affect the gradients from the FSS probes e.g. Run 6. Figure 6 also shows 1 minute averages of liquid water content obtained from probe 2 for the first five runs. The slow response is evident for instances when large changes in liquid water content occur. These effects were particularly evident for runs 7 to 10 as a result of low liquid water content and possible evaporation effects.

9 Variation of Deposition Velocity with Droplet Size

Each size class was treated in a similar manner to the histogrammed liquid water content data from each probe, using the channel by channel normalisation values shown in Figure 3. Table 4 shows the results from run 3. This run was typical for periods where the liquid water content at 1 m was between 0.13 and 0.17 g m^{-3} i.e. runs 3,4,5 & 10. To compare the variation from run to run the deposition velocity was normalised using the momentum deposition velocity as shown in Figure 7.

The relationship between deposition velocity and drop size showed consistent behaviour from run to run. The deposition velocity (V_d) increased with particle size within the size range 2.5 to 6.5 µm, from about 10 mm s

IC

$^{-1}$ to 50 mm s^{-1} . At about 6.5 µm droplet radius the deposition velocity is approximately equal to the deposition velocity for momentum V_m (Figure 7). The small droplets (2.5-5.0 µm) are not captured at the surfaces of the vegetation as efficiently as momentum, which is transferred by skin friction *and form* drag in droplet deposition velocity, and the gradual increase reflects the increasing efficiency of impaction processes as the mass of the droplet increases, Chamberlain (1975). The observed deposition velocity increases to values greater than V_m for the size range 6.5 to 10.5 µm radius after which a sharp decline is observed for 10.5 to 15.5 µm droplets. For the size range 12.5 µm to 15.5 µm, droplet deposition velocities are smaller than V_m, although the error bars for these droplets are very large.

10 Chemical Deposition

Samples of the cloud water were collected and stored in a refrigerator at 4 ^{0} C for later analysis by ion-chromatography. Using the liquid water fluxes from Table 2 the chemical deposition rate for the chemical agent was calculated .This is shown in Table 5.

11 Discussion

The experiments have shown that at Great Dun Fell the deposition velocity of cloud liquid water to the hillside is close to the value of momentum. This is in broad agreement with the results of Dollard *et al.* (1983). The measured chemical agent deposition rate was 1 mg m^{-2} hr^{-1} . This may be compared with values typically 3-6 mg m^{-2} hr^{-1} reported by Choularton *et al.* (1988) due to rainfall when the seeder-feeder mechanism is operating. The direct deposition of cloud droplets is unlikely to contribute a major fraction of the water deposited to a hillside. The mean annual wind speed, computed over a 10 year period, for Great Dun Fell is 11 m s^{-1} at 10 m above the summit. With 226 days of cloud per year each of 4 hours duration this would give between 50 and 130 mm of water deposited to the hill by cloud compared to typically 2000 mm by rain. However, because the total duration of in cloud conditions for hills such as Great Dun Fell is much greater than the duration of rainfall, the deposition of chemical species by turbulent deposition is at least comparable to that for rainfall at high altitude. Between the period 1972 and 1979 Great Dun Fell was in cloud for parts of 226 days per year

compared to 153 rain days. This would result in cloud deposition duration typically 5 to 10 times that for rainfall

The concentrations of all chemical species are generally much higher in cloud water than in rain water Fowler *et al* (1988). The data presented above also show that when the cloud is thin the lysimeter may show a net weight loss despite a significant downward flux of cloud water deduced by the gradient technique. This suggests that vapour deficit at the wet surface is causing evaporation of the water on the affected surfaces and provides experimental support to the suggestion made by Unsworth (1983) that simultaneous turbulent deposition and evaporation of water from the effected surfaces will result in enhanced concentration of chemical species on the surfaces .

The data presented in this paper have for the first time demonstrated the size dependence of the deposition velocity of cloud droplets over a natural surface. The increase in deposition velocity between droplet radii of 2.5 and 6.5 μm may be attributed to the reduction of the surface resistance in this range. These results are consistent with the model predictions of Slinn (1982) for solid particles It is difficult to model such effects accurately due to factors such as sheltering coefficients , e.g. Underwood (1987). Droplets between 6.5 and 10.5 μm radius exceed the momentum deposition velocity due to increased efficiency of collection by impaction to the surface. Above 10.5 μm a sharp decrease in deposition velocity occurs for radii up to 15.5 μm (the largest size measured). This effect is difficult to quantify due to the large sample errors in the data for this size range but is qualitatively consistent with bounce off effects predicted for solid particles in a similar range range and observed by Chamberlain (1967). The data may suggest that droplets in this size range are not being efficiently captured by the surface. This effect, however, is not likely to become important as in this size range sedimentation velocities are beginning to become important and will clearly dominate for still larger droplets. More work is required to quantify these effects.

The results obtained here suggest that the model of Hill *et al* (1987) may be used to give reasonable estimates of turbulent deposition rates to hills . They assumed that the droplet deposition velocity was equal to that for momentum. This assumption is only in error for very small droplets of radius < 5 μm. This size will be achieved within 100 m of cloud base on hills in maritime locations where occult deposition is common. More detailed calculations including surface resistance effects will be required in regions

frequently subjected to different CCN distributions where large numbers of very small droplets are present.

Acknowledgements

We would like to thank Dr R.L.Hall of the Institute of Hydrology, Oxon, for the loan of and advice in using the lysimeter. Various members of the UMIST Atmospheric Physics Group contributed advice and expertise particularly in the use of the FSS probes, for which we thank them. Dr D.J.Carruthers from the University of Cambridge gave advice in the analysis and interpretation of the data. This work was funded by the Electrical Power Research Institute (USA), the Central Electricity Generating Board (UK) and the Department of the Environment (UK). A.P.Morse acknowledges receipt of a NERC research studentship.

Table 1

Run No.	Time O.M.T.	U* m/s	Zo mm	d cm	L(1.0 m) mg/m3	R µm	wind direction	Flux mg/m2/s	Vt mm/s	Vm mm/s	Vd mm/s	Vt/Vm
2	00:34-00:54	0.56	12	7	90	5.4	NE	6.0	63.2	51.8	67.0	1.22
3	00:54-01:10	0.59	11	7	164	6.2	NE	10.0	55.5	53.5	60.6	1.04
4	01:10-01:25	0.58	11	7	133	5.8	NE	7.7	53.6	52.6	58.0	1.02
5	01:25-01:40	0.56	11	7	167	6.1	NE	8.9	48.7	51.2	53.5	0.95
6	01:40-01:55	0.55	11	7	240	6.6	NE	10.1	36 6	50.1	42.2	0.73
7	01:55-02:10	0.55	11	7	107	5.6	NE	5.8	50.4	49.0	54.5	1.03
8	02:10-02:25	0.58	11	7	13	4.2	NE	*	*	*	*	*
9	02:25-02:40	0.55	15	7	98	5.0	NE	5.9	57.5	54.1	60.8	1.06
10	02:40-02:55	0.55	13	7	153	5.0	NE	7.5	45.3	52.1	48.6	0.87

Table 2 Comparison of total water flux and measured by the lysimeter and Gradient techniques.

Run	Fw Lysimeter Flux mg m^{-2} s^{-1}	Fc Cloud Flux mg m^{-2} s^{-1}	Fw/ Fc
2	2 ± 4	6.0 ± 0.5	0.3
3	20 ± 6	10.0 ± 1.0	2.0
4	9 ± 7	7.7 ± 0.7	1.2
5	- 4 ± 5	8.9 ± 0.9	-0.4
6	31 ± 6	10.1 ± 1.4	3.1
7	- 2 ±10	5.8 ± 0.8	-0.3
8	- 4 ± 9	1.8 ± 0.2	-2.2
9	8 ± 5	5.9 ± 0.5	1.4
10	4 ± 5	7.5 ± 0.7	0.5

Table 3 : Deposition velocities calculated from Run 5 as a function of size

Radius μm	V_t mm s^{-1}	error %	V_d mm s^{-1}	V_t / V_m
2.5	5	66	5	0.09
3.5	38	8	40	0.71
4.5	27	8	29	0.50
5.5	42	5	46	0.79
6.5	54	2	58	1.01
7.5	45	4	51	0.84
8.5	62	4	71	1.16
9.5	68	4	79	1.27
10.5	76	4	89	1.42
11.5	69	7	84	1.29
12.5	47	16	66	0.88
13.5	42	42	64	0.79
14.5	23	59	49	0.43
15.5	22	98	51	0.41

Table 1

Mean Flux of chemical Agent.

Cloud Water Collection 00:27 - 01:55 Runs 2-5

Measured Concentration of Chemical Agent : 322 µlgl l-1

Mean Chemical Agent Flux to surface : 1.1 mg m-2 sec-1

References

Calder I.R., Hall,R.L., Harding R.J. & Wright I.R. (1984) The Use of a Wet-Surface Weighing Lysimeter in Rainfall Interception Studies of Heather (*Calluna vulgaris*). *Jof Climate & Applied Meteorology* Vol 23 pp 461-463.

Chamberlain A.C. (1967) Transport of *Lycopodium* spores and other small particles to rough surfaces. *Proc.R Soc.* 296A, 45-70.

Chamberlain A.C. (1975) The movement of particles in plant communities. *in Vegetation in the Atmosphere* Edited by J.L Monteith pp.155-203. *Acad Press* 1975.

Chandler A.S., Choularton T.W., Dollard G.J.,Gay M.J., Hill T.A., Jones A., Jones B.M.R.,Morse A.P., Penkett S.A. & Tyler B.J. (1988) A field study of the cloud chemistry and cloud microphysics at Great Dun Fell *Atmospheric Environment* (In Press)

Choularton T.W., Consterdine I.E., Gardner B.A., Gay M.J., Hill M.K., Latham J. & (1986) Field studies of the optical and microphysical characteristics of clouds enveloping Great Dun Fell *Quart.J.Roy.Met.Soc* Vol. 112 No. 471 pp 131-148.

Stromberg I.M.

Choularton T.W. (1988) Gay M.J., Jones A., Fowler D., Cape J.N. & Leith I.D., The influence of altitude on wet deposition : comparison between field measurements at Great Dun Fell and the predictions of a seeder-feeder model. *Atmospheric Environment* (In Press).

Consterdine I.E. (1984) Infra-red Transmission in Limited Visibilty Conditions. Ph.D. Thesis. *University of Manchester*

Dollard G.J., Unsworth M.H. & Harvey M.J. (1983) Pollutant transfer in upland regions by occult precipitation. *Nature* Vol. 302, pp 241-243.

Dollard G.J. & Unsworth M.H. (1983) Field Measurements of turbulent fluxes of wind-driven fogs to a grass surface. *Atmospheric Environment* Vol 17, No. 4, pp 775-780.

Fowler D., Cape J.N., Leith I.D., Choularton T.W., Gay M.J. & Jones A. (1988) The influence of altitude on rainfall composition. *Atmospheric Environment* (In Press).

Gallagher M.W., Choularton T.W., & Hill M.K. (1988) Observations of airflow and turbulence over a large hill of moderate slope. *Boundary Layer Meteorology* Vol.42 No 3

pp. 229-250

Hill T.A., Jones A. & Choularton T.W. (1987) Modelling sulphate deposition onto hills by washout and turbulence. *Quart. J Roy Met Soc* Vol. 113. No. 478 pp 1219-1236

Kerfoot, O. (1968) Mist Precipitation on Vegetation. *Forestry Abstracts* Vol 29. pp 8-20.

Latham J., Blyth A.M. & Chittenden A.M.I. (1984) An optical novel device for measuring liquid water content in clouds. *Proc. IX Int Conf on Cloud Physics, Tallinn* pp 765-767

Milne,R. Crossley,A. & Unsworth,M.H. (1988) Physics of cloud water deposition and evaporation at Castlelaw, SE Scotland. *Proceedings on the NATO Conference on Acid Deposition Processes at High Elevation Sites Edinburgh (1988)*

Nagel J.F. (1956) Fog Precipitation on Table Mountain. *Quart. J Roy Met Soc* Vol. 82. pp 452-460

Slinn W.G.N. (1982) Predictions for Particle Deposition to Vegetative Canopies. *Atmospheric Environment* Vol 16. No. 7. pp 1785-1794.

Unsworth M.H. (1984) Evaporation from forests in cloud enhances the effects of acid deposition. *Nature* Vol. 312. pp 262-264.

Underwood, B.Y. (1987) Dry deposition to a uniform canopy : Evaluation of a first-order-closure mathematical model. *Atmospheric Environment* Vol 21. No. 7. pp 1573-1585.

Legends to Figures

Figure 1. The experimental arrangement showing : Scaffold tower with FSSP's; Profile anemometer tower; Lysimeter; and the Instrumented Vehicle & Generator.

Figure 2. Histogram of number concentration (cm^{-3}) versus radius (μm) for a typical in cloud period observed by the FSSP mounted at 3.5 m .

Figure 3. The normalisation factor R derived from running both probes side by side with the mean error for all runs as a function of droplet size.

Figure 4. Trace showing 1 minute averages of liquid water content calculated from droplet spectra observed by FSSP 2 at 3.5 m for the morning of 11/6/87.

Figure 5 Wind profile measured at 4 levels for Run 5 on 11/6/87.

Figure 6. The variation in liquid water content obtained from the FSSP (dark line) and the mass of the lysimeter (dashed line) from 00:00 to 02:00 GMT (runs 2 to 5).

Figure 7. Deposition velocity normalised by the momentum

deposition velocity, $\frac{V_t}{V_m}$, as a function of droplet radius for runs 3,4,5 & 10 on 11/6/87.

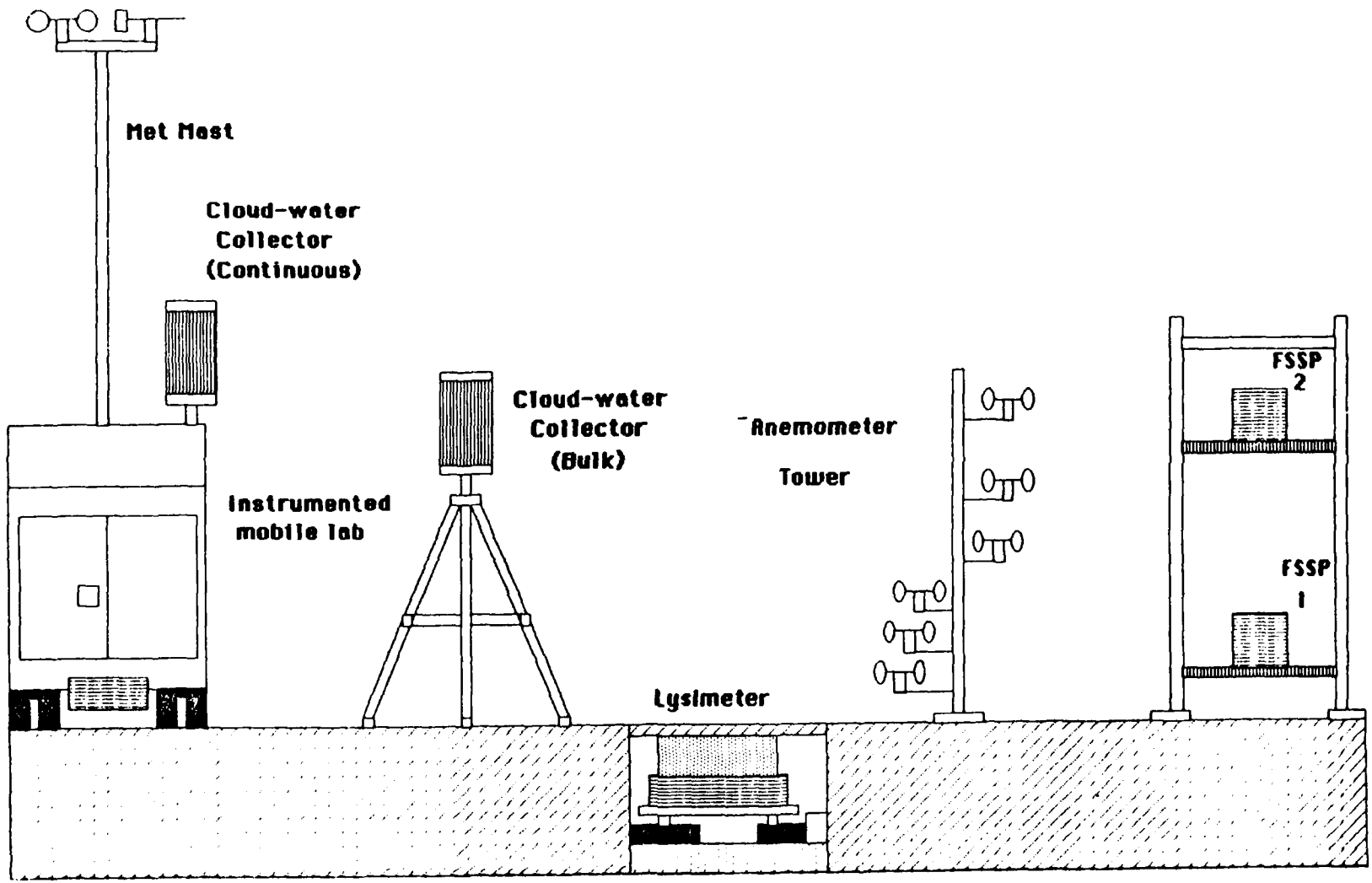
Met Mast
Cloud-water
Collector
(Continuous)
Instrumented
mobile lab
Cloud-water
Collector
(Bulk)
Anemometer
Tower
FSSP
2
FSSP
1
Lysimeter

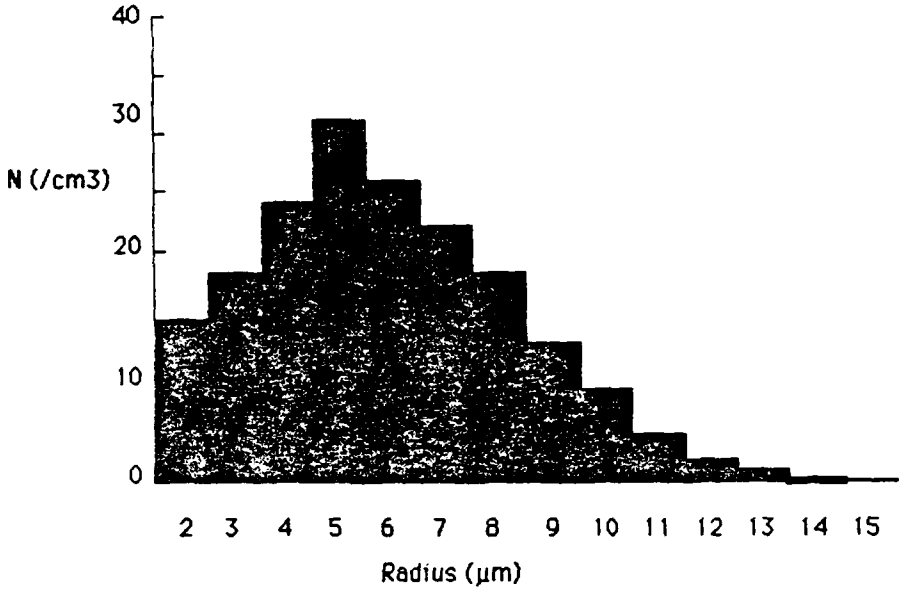
40
30
20
10
0
N (/cm3)
2 3 4 5 6 7 8 9 10 11 12 13 14 15
Radius (μm)

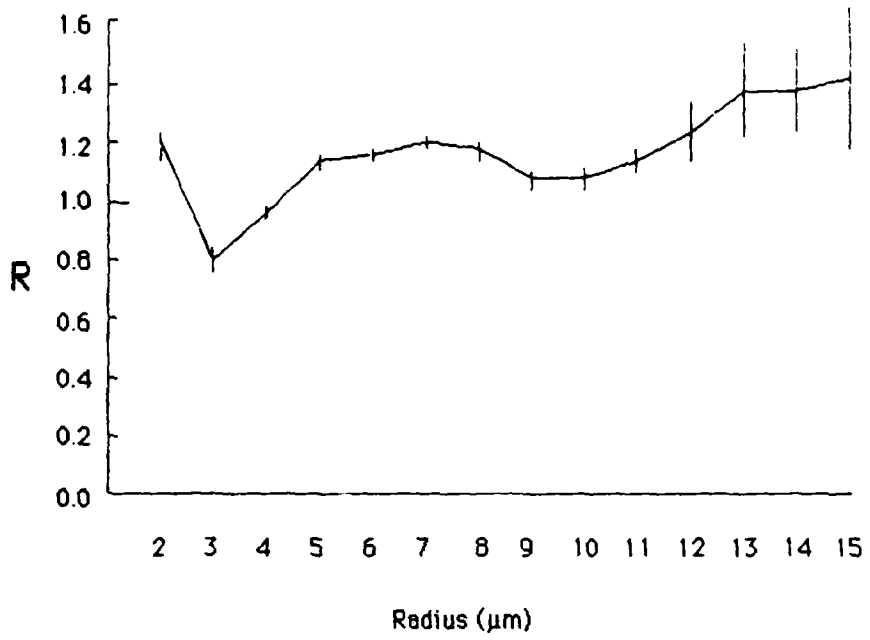
1.6
1.4
1.2
1.0
0.8
0.6
0.4
0.2
0.0
R
2 3 4 5 6 7 8 9 10 11 12 13 14 15
Radius (μm)

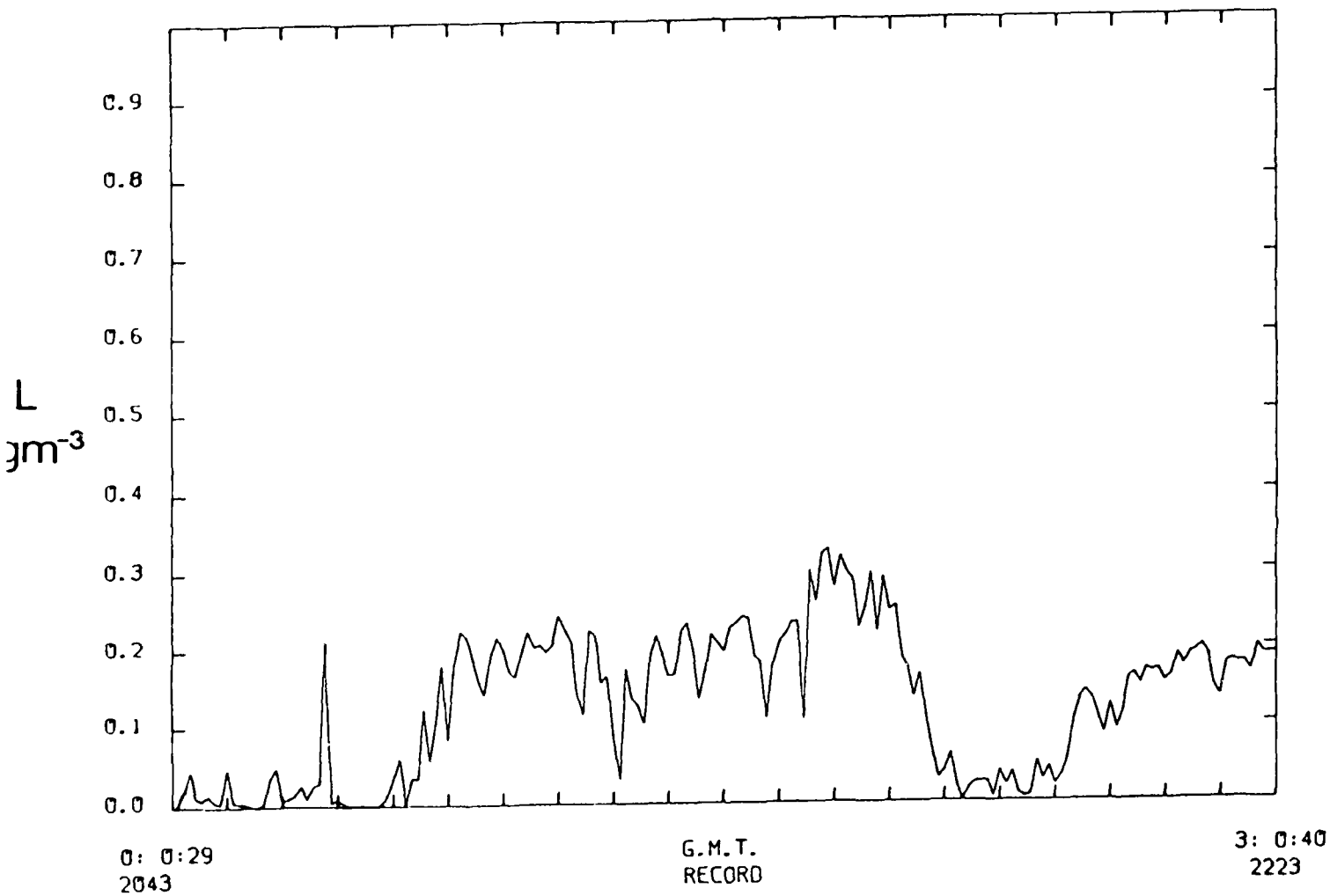

Figure 5

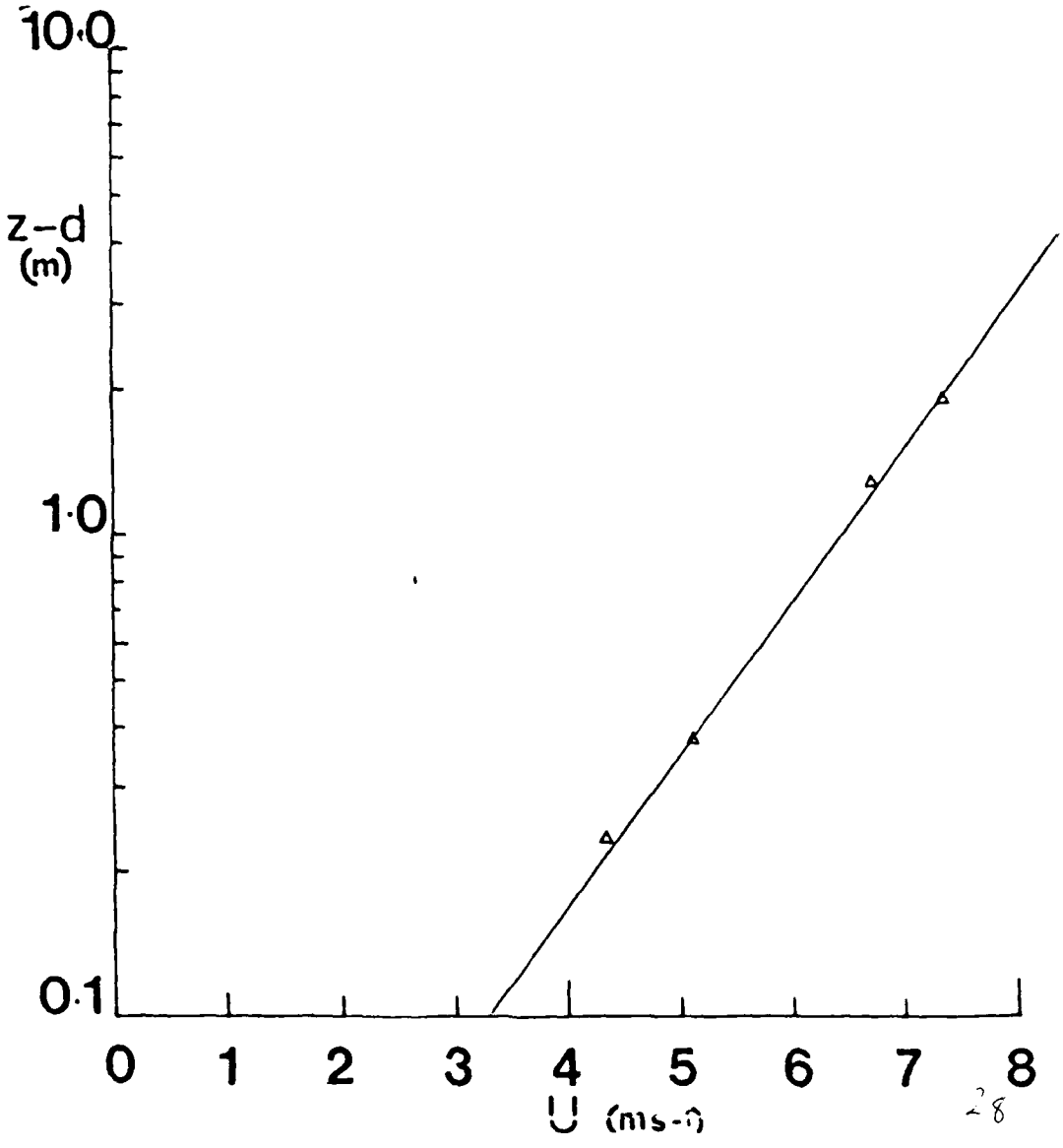
10·0
z–d
(m)
1·0
0·1
0
1
2
3
4
5
6
7
8
U (ms-1)

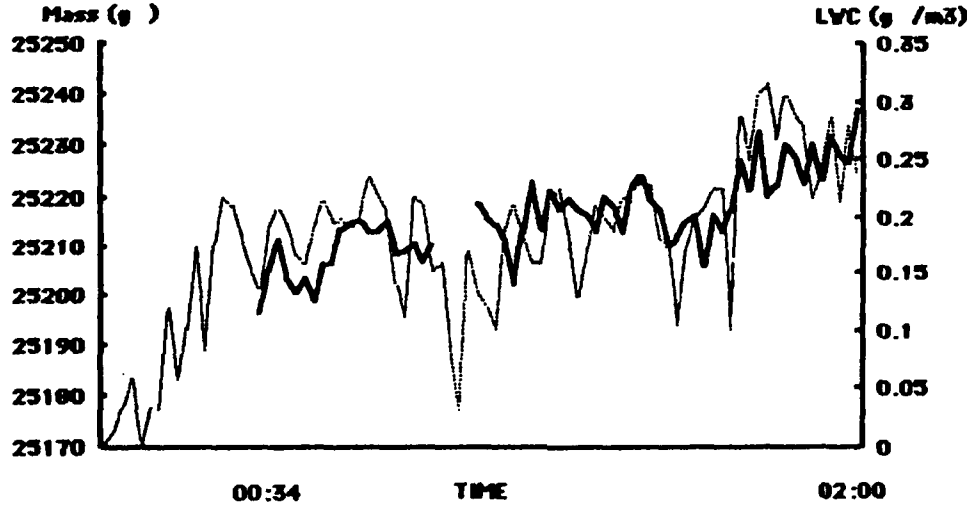
Mass (g)
LWC (g /m3)
25250
25240
25230
25220
25210
25200
25190
25180
25170
0.35
0.3
0.25
0.2
0.15
0.1
0.05
0
00:34
TIME
02:00

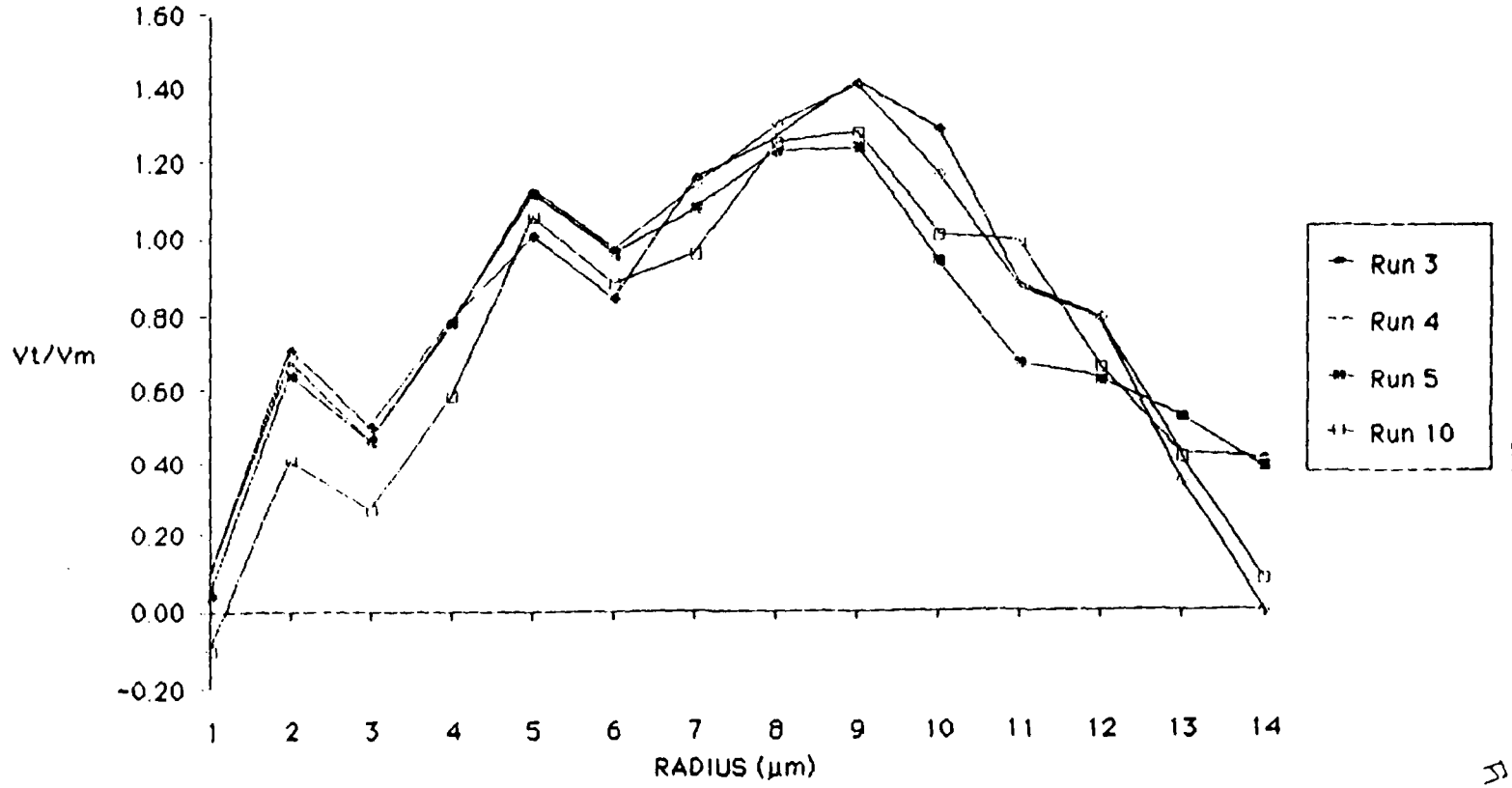
1.60
1.40
1.20
1.00
0.80
0.60
0.40
0.20
0.00
-0.20
Vt/Vm
1
2
3
4
5
6
7
8
9
10
11
12
13
14
RADIUS (µm)
Run 3
Run 4
Run 5
Run 10

Section 3

MODELLING THE DEPOSITION OF CHEMICAL AGENTS BY WASHOUT AND TURBULENCE

Abstract

It has recently been shown from model predictions and measurements at Great Dun Fell, U.K, that the variation of chemical agent deposition with altitude associated with rainfall is much larger than had previously been thought. In this paper the model of deposition by the seeder-feeder mechanism is extended to cover a wider range of atmospheric conditions and hill sizes and the results are compared with a model of turbulent deposition . It is shown that turbulent deposition rates are about a factor of 5 to 10 less than the seeder-feeder mechanism. The patterns of both types of deposition are strongly affected by atmospheric stability and windspeed. The model of deposition by washout of a hill cap cloud by rain predicts that for a steep hill, characteristic length 2 km, the maximum rainfall and chemical agent deposition rates are downstream of the hill summit. In this case, the raindrop trajectory through the highest liquid water content region is short, but the condensation rate is large due to strong updraughts. Hence the greatest effect is the wind-drift of the raindrops and consequently the rainfall and deposition maxima are displaced downstream. On a longer hill, about 10 km in length, cloud water is not so rapidly resupplied due to reduced updraught. The rainfall rate in the region of the summit is greater than for a steep hill because the region of high water content is large in horizontal extent and the effects of wind-drift are small. As a result, the maximum rainfall and deposition rates occur

somewhat upstream of the hill summit, depending on atmospheric stability.

1. Introduction

In this section of the report we describe a model of the deposition of chemical agents to elevated topography by the direct turbulent deposition of cloud droplets from the cap cloud to the surface and washout by the seeder-feeder process.

2. Cap Cloud Model and turbulent deposition

This model is a development of that described in Hill et al 1986 and so it will only be outlined here. In order to calculate the chemical agent concentration in the droplets at a particular point on the hill side we require a representative transit time from cloud base to a measuring site on the hill surface. We therefore firstly require an airflow model of the hill. The wind velocities need to be predicted close to the hill surface with some accuracy as well as throughout the cloud depth because all measurements are made within 10 metres of the ground. We use the model of Carruthers and Choularton 1982 which was developed specifically for Great Dun Fell and which has received experimental verification at this site.

We solve Helmholtz's equation for inviscid flow

$$\nabla^2 \zeta + \mu_i^2 \zeta = 0$$

where μ_i is the Scorer parameter N_i / U_i in layer i.

and U_i is the geostrophic wind. ζ is the streamline displacement.

and use f(x) as the lower boundary condition where

$$f(x) = \frac{H}{\left(1 + x^2/L^2\right)}$$

H is height of hill and L half width at half height.

The buoyancy frequency N_i is defined as

$$\left(\frac{g}{\theta_i}\frac{d\theta_i}{dz}\right)^{1/2}$$

where θ_i is the mean potential temperature of the layer and g the acceleration due to gravity.

The atmosphere may be divided up into several layers and this is important because the stability of the air above the turbulent boundary layer can have a large effect on the flow of air in this lowest layer (the layer in which the cloud frequently resides).

Close to the hill surface the Reynolds stress and viscous terms cannot be left out of the momentum equation and therefore in the region just above the ground the wind velocities are calculated by the method described in Jackson and Hunt 1975. It is not proposed to discuss this model in detail here. It has recently been suggested by Mason 1986 that

the inner layer depth within which the turbulence is in local equilibrium may be significantly smaller than suggested by Jackson and Hunt. Measurements of the wind profile using a 3m tower of precision anemometers and other anemometers at 3m and 10m above the terrain on the summit, together with measurements of the turbulence using a Sonic Anemometer have been made at Great Dun Fell (Gallagher et al 1987). These measurements show that the inner layer depth is about 30m with the turbulence close to local equilibrium in the lowest 10m at least. All of the hills discussed below have inner layer depths at least as large as GDF. Nearly all the depletion in cloud droplet concentration occurs well within this depth and so this has no significant effect on the discussion presented below.

Given the wind field over the hill surface, the next step is to incorporate the cap cloud. In this model the cloud either begins when the rising air has cooled to saturation or we can specify cloud base as occurring at some height based on observation. The depth of the cloud is estimated from soundings in the vicinity of the hill. The density changes due to release of latent heat during the condensation process are insufficient to alter the dynamics for a hill of this size.

The position of any streamline and the wind velocity along any point of it can be calculated and used to find the liquid water content and droplet size distribution variation over the hill using the standard droplet growth equations. Hence we can produce droplet size distributions and droplet composition concentrations for a given position on the hill. We are, in effect, employing a lagrangian parcel model at this stage (containing the microphysics) and following its development as it is driven over the hill by the wind-field determined as described above.

The concentration of chemical species may be allowed to vary within the collection of droplets according to the equations set out in section 2. and gases exchanged between the droplets and the surrounding air. For the purposes of this paper the details of the chemistry associated with a particular droplet class are not important and the mass of eg. chemical agent deposited is determined from the total mass present at a given time. The bulk concentrations of the various ions are, however, determined by integration of ten droplet size categories. The droplet growth equations used may be found in Hill and Choularton 1986.

The boundary layer in which the cap cloud resides is turbulent so that droplets tend to mix vertically during transit. The approximate distance through which a droplet will move in time Δt is given by $U_* \Delta t$ where U_* is the friction velocity. Given the approximate transit time of cloudy air from cloud base to the point of measurement, also Δt, we can arrive at a vertical distance such that droplets throughout this depth will have an equal chance of being intercepted at the measuring site.

Figure 1 shows schematically one such region of cloud that this argument defines, stretching back upstream from a particular point on the hill towards cloud base. An average cloud parcel trajectory can now be calculated and hence a vertical wind profile for use in determining droplet growth.

Knowing the composition of the cloud which is in contact with the hill allows us to estimate the turbulent deposition rate of a chemical species to the hill surface of known roughness length at a given position, A. We solve

$$K(z)\frac{dC(z)}{dz} + V_t C(z) = V_d(z)C(z) = \text{constant}$$

Where $C(z)$ is the droplet concentration and $V_d(z)$ their deposition velocity. $K(z)$ is the eddy diffusivity = KzU_*, and the droplet terminal velocity $V_t \ll U_*$ and U_* is defined by

$$U(z) = \frac{U_* \ln(z/z_o)}{K}$$

K is the van Karman constant.

Solving for $V_d(z)$ at a point A, assuming the droplet flux is independent of height near the ground, gives

$$V_d(z) = \frac{U_{*A}}{\ln(z/z_o)}$$

In the absence of detailed experimental data to the contrary we assume that the deposition is limited by turbulent diffusion. This is likely to be a reasonable assumption since the average size of the cloud droplets is 5 to 10 μm unless we are very close to the region of cloud base near the hill surface. The liquid water content at A is calculated assuming no depletion (ie. z must be > 10m if z_o = 0.02 m) and hence we use the concentrations predicted by the model 10m above the ground. If z_o = 0.5m, corresponding to a forested hill, then z = 25m. U_* is about $1ms^{-1}$ for windspeeds of $15ms^{-1}$ employed by the model and hence an insignificant fraction of time is spent by droplets in this region compared with the

transit time over the hill, consequently the existence of the depletion zone will not affect the chemistry of the deposited droplets.

3. Results of the Turbulent Deposition Model

Table 4 presents a set of standard conditions used as input to the model. The input parameters are typical of values measured at Great Dun Fell and the stability parameters chosen give a supercritical airflow regime characteristic of hills whose height is comparable to the boundary layer depth. The hill height of 665m chosen corresponds to the height of GDF above local terrain. The hill half length L of 2 km corresponds to GDF and 10km to a longer hill.

The Great Dun Fell hill is grass covered and experiment has suggested that a roughness length of 2 cm is appropriate. However, this can be changed in the model in order to describe other terrain eg. a forested hill. The rate of deposition will be higher over such a surface if z_o is taken as 50 cm for such a hill. This assumes that all the terrain in the model domain is forested so that turbulent diffusion delivers the droplets to the tree tops where they are intercepted. If a transition in the surface properties occurred, eg from grass to forest then locally enhanced deposition would occur due to interception at the forest edge and the turbulence would be disturbed for a short distance downwind while it adjusted to the higher roughness. These complications are not treated in this paper.

The Short Hill

In figures 2a and 2b curve a shows the occult precipitation rate and chemical agent deposition rates respectively for a short hill. It can be seen that the precipitation rate increases toward the hill top as the liquid water content and windspeed increase. The airflow regime is supercritical and consequently the deposition velocity continues to increase on the lee-side of the hill. This does not, however, produce any marked shift in the maximum 'occult' precipitation rate away from the summit because the water content decreases as the cloud moves down the lee-side. The chemical agent deposition rate, though, continues to increase across the hill as the windspeed increases, this process being independent of the cloud liquid water content above cloud base (where the deposition is assumed to be limited by turbulent diffusion). Doubling the windspeed (curves b) roughly doubles the deposition rates as the total depletion of the cloud is very small. Raising cloud base to 500m considerably reduces the precipitation rates by reducing the cloud liquid water content but does not affect the chemical agent deposition rates except by reducing the part of the hill enveloped by cloud (the deposition rates of sub-cloud aerosol are assumed to be small due to surface resistance). Increasing the chemical agent aerosol loading proportionately increases the deposition rate, curve d. Curve e shows the effect of a totally neutrally stable atmosphere. The major effect of this is to reduce the windspeeds on the lee-side of the hill and hence reduce the deposition rates there.

Curve g shows the effect of simulating a forested hill with a roughness length of 0.5m. This results in an increase in the deposition rates of 2.5 to 3 times on the short hill. The depletion of chemical agent and liquid water are still small

In order to illustrate the effect of changes in atmospheric stability we show the results of weakly stable upper air and a neutral atmosphere with symmetrical flow (figure 3). It can be seen that the stability of the upper layers is important in determining the deposition rate especially on the lee-side. Different atmospheric conditions can result in differences of a factor of 2.

The Long Hill

Figures 4a and 4b show the occult precipitation rates and chemical agent depositions over the hill with L=10km. The curves correspond to those of figures 2a and 2b. The pattern of results is very similar to the short hill case with some exceptions. The deposition and precipitation rates are not as high in the long hill case for potential flow (curve e), particularly near the hill top and on the lee-side because the speed-up of the wind is significantly reduced due to the larger aspect ratio (see Carruthers and Choularton 1982). However in supercritical flow regimes the pattern is more complex with larger deposition rates well downstream of the summit.

A further effect is that for the depths of cap cloud chosen (400 and 800m), and when the hill is forested, with a roughness length of 0.5m, a

significant depletion of both liquid water and chemical agent occurs. This means a reduction in deposition rate especially downwind of up to about 60% and 30% respectively when this is allowed for. In order to simulate this depletion we remove a fraction , F ,of droplets per time interval, Δt, given by

$$F = \frac{V_d \cdot \Delta t}{H_c}$$

Where H_c is the depth of the cloud. We assume implicitly that turbulent mixing occurs through the depth of the cloud in a time short compared with the transit time. In all other cases discussed above, the depletion of the cap cloud is small and so its vertical depth does not play a significant role.

The effect of increasing the aerosol chemical agent loading is to increase the deposition rate proportionately everywhere over the hill.

4. Washout Model

The other process by which cloud water is deposited onto the hill surface is rainfall. Because the average droplet lifetime in deep cap cloud is typically ten to twenty minutes there is insufficient time to generate precipitation sized droplets by coalescence. Instead any rainout is likely to be due to the sweeping out of droplets by rain falling from higher level cloud often associated with a front. This process is frequently referred to as the 'seeder-feeder' process, Bergeron 1965. The rainfall rate will therefore be enhanced over the surface of the hill

and the enhancement will be related to the path of the raindrops falling through the cloud - being proportional to the liquid water content integrated along the path. The model is based on that of Carruthers and Choularton 1983. The concentration of aerosol chemical agent upwind of the hill is specified and assumed to be independent of height through the depth of the feeder cloud. This may sometimes be unrealistic especially when the cap cloud extends into the inversion layer as discussed below. When the cloud forms it is assumed that all of the chemical agent is incorporated into the cap cloud droplets by nucleation scavenging. Typical cloud base updraughts for this model are about 1ms ' and under these circumstances most aerosol size categories are activated suggesting that in this case this assumption is valid. The details of the washout model are presented in Carruthers and Choularton(1983). It has been modified here to include calculations of the washout of the chemical agent and is outlined below.

The air within the depth of the feeder cloud is covered by a streamline following grid. If the air following a particular streamline is initially below the height of cloud base no condensation or chemical agent scavenging takes place until it has been displaced vertically to the height of cloud base. Condensation along streamlines initially above cloud base starts as soon as they suffer a vertical displacement. The rainfall rate from the seeder cloud together with its chemical agent concentration is specified and the raindrop size distribution is assumed to follow a Marshall- Palmer distribution (the model has also been run using a Best distribution for the seeder cloud raindrop spectrum but this does not affect the results significantly see Carruthers and Choularton 1983). This rain falls into the top of the feeder cloud.

Starting at the most upstream element of the top row of the grid the liquid water content increase is calculated as the air parcel travels adiabatically across the grid. This liquid water is depleted by the scavenging of the cloud droplets and the chemical agent they contain by the raindrops, with a collection efficiency close to unity as the air parcel travels across the grid element. Hence the nett change in the liquid water content and the depletion of chemical agent across the grid element may be calculated. This process is repeated along the top row of the grid.

The increase in radius and chemical agent concentration in each raindrop size category is calculated from the amount of cloud water scavenged as the raindrop falls vertically through the grid element. The windspeed and terminal velocity of the droplets are used to calculate the drift of each drop size category during this process and the droplets are moved downstream and allocated to the appropriate grid element of the next row down.

The whole process described above is repeated until the raindrops reach the hill surface. It is assumed that the scavenging of chemical agent is negligible for liquid water contents of less than $0.02g\ m^{-3}$. The results are insensitive to this figure. All nucleation scavenging will take place rapidly whilst the liquid water content is of this order and below this value droplets will exist as unactivated aerosol for which the collection efficiency by raindrops is very small.

A steady-state situation is envisaged in which cloud is being continually swept out by the rain and replaced by fresh cloud due to condensation in the air flowing over the hill. The path of the droplet is determined by its fall speed and the flow speed of the air over the

hill. There are therefore two main factors which determine the deposition pattern . Firstly, there is the path length of the rain drop, determined by the hill length and the wind velocity and secondly the rate at which water depleted by the washout process is replaced by condensation. The condensation rate is determined by the updraught speed and consequently hills of greater aspect ratio and hence higher vertical winds close to the summit will have associated cap clouds which are not so seriously depleted of water close to the summit. We can summarize these arguments in terms of two length scales:

The horizontal drift of a raindrop radius r falling at speed V_r through a cloud of depth Z_c

$$L_d \simeq \frac{Z_c U_o}{V_r}$$

The scale length of horizontal variation in liquid water content q

$$L_q \simeq \frac{q}{\left(\frac{\delta q}{\delta x}\right)} \simeq L$$

Where L is the half length of the hill. For a short hill, $L_d \ll L_q$.

5. Results of the Model of the Seeder-feeder effect

a. The Rainfall Distribution

To illustrate these effects figures 5a and 5b show the rainfall distribution patterns for the case of a short hill (applicable to Great Dun Fell) characteristic length 2km and for a long hill , length 10km. Other parameters are varied as for the occult precipitation discussed above.

When the hill is steep, figure 5a, the trajectory of the raindrops through the highest water content region is relatively short but the condensation rate is large due to the large vertical winds. Hence the greatest effect is wind-drift and the maximum rainfall rate is displaced downstream. For a supercritical flow regime (curve a), the maximum enhancement is about 10% larger, and slightly nearer the summit, than for potential flow (curve b). The effect of wind-drift is markedly reduced by a lower windspeed (curve c), or a shallower cap cloud (curve d), which also has the effect of reducing the rainfall enhancement.

Higher windspeeds (curve e) tend to reduce the maximum enhancement, while increasing the distance downstream over which enhancement occurs. A higher rainfall rate (curve f) does not increase the enhancement pro-rata as the raindrop sizes also increase.

In the case of the longer hill, Figure 5b, cloud liquid water scavenged is not so rapidly resupplied due to the reduced updraught. In the region of the summit, the rainfall rate is greater than for a steep hill because the maximum liquid water content region is relatively large in horizontal extent and the effects of wind-drift small. The maximum enhancement occurs slightly upstream of the summit for the

supercritical flow regime (curve a) and near the summit for potential flow (curve b). The enhancement under supercritical flow is also about 15% less than for potential flow.

A shallower cap cloud reduces the enhancement markedly (curve c), whereas a higher windspeed (curve d) increases the enhancement due to higher vertical winds and larger condensation rate in the feeder cloud.

The effects on enhancement of a high rainfall rate (curve e) is less than for the steep hill due to the lower cap cloud liquid water content.

b. The Deposition of Chemical Agents

If we now consider the deposition of the aerosol chemical agent dissolved in the cloud water then the patterns for the short and long hills are represented in figures 6 and 7. It is immediately apparent that the deposition rates are 5X to 10X higher than the corresponding occult deposition rates

For the short hill, figure 6 the deposition curves peak downwind of the summit. The changes in deposition patterns due to varying physical parameters, closely follow the distribution of rainfall enhancement. This is because, in each case only a small proportion of the chemical agent in the cloud is washed out. Increasing the seeder cloud precipitation rate to 5mm h^{-1} (curve e) increases the peak deposition rate from 4.4 mg $m^{-2}h^{-1}$ to 17.6 mg $m^{-2}h^{-1}$ and slightly changes the distribution of the deposition due to the larger raindrops associated with the higher rainfall rate.

For the long hill, figure 7, there is a faster decline in deposition rate downwind of the hill (eg. curves a). This is because, although the water content is maintained to some extent by condensation on the upwind side, the aerosol chemical agent is not replenished and hence declines continuously with position on the hill. This becomes a significant effect on the long hill because of the longer transit times of air parcels through the feeder cloud. Again it can be seen that, in the absence of chemical agent production, increasing the aerosol chemical agent loading entering cloud base or increasing the seeder rainfall rate (figure 7a, curve e) has the most dramatic effect on the deposition pattern. Increasing the seeder cloud rainfall rate to 5mm h^{-1} increases the peak deposition rates from 4.0 to 14.2 mg m^{-2} h^{-1}, smaller than for the short hill due to the higher total chemical agent scavenged.

A potential flow regime, (figure 7, curve b), tends to produce a more symmetrical deposition pattern while a higher windspeed, (figure 7b, curve c), increases the peak deposition slightly, and also shifts the peak more towards the summit.

6. Discussion

The object of this paper was to compare occult and rainfall deposition rates under similar conditions. Results show that precipitation by the seeder-feeder process is 5-10 times as efficient if typical concentrations of chemical agent and rainfall rates as measured in the U.K are used. Many hills, however, are enveloped by cloud for much longer periods than the total duration of rainfall and so 'occult'

deposition can make a substantial contribution to the total chemical agent deposition.

The results presented above have shown that occult precipitation rates are predicted to be a maximum close to the hill top but with a supercritical airflow regime, characteristic of hills with a comparable height to the boundary layer depth, the chemical agent deposition rates are a maximum on the lee side of the hill for both long and short hills. (It should be noted that the area over which material is deposited is much less than when the washout process is operating.)

A forested hill has a deposition rate 2.5 to 3 times higher than on a grass covered hill. This is reduced somewhat over a long hill where depletion of the cloud by the deposition may be important.

The pattern of deposition during rainfall is much more strongly dependant on hill size. On the short hill the peak deposition rate and rainfall occur downwind of the hill summit due to the important effects of wind-drift. On the long hill the peak rainfall and deposition rates occur at or somewhat upwind of the hill summit. Maximum deposition rates tend to be somewhat smaller than on the short hill due to depletion of the feeder cloud by the scavenging, although the total deposition on the hill is considerably larger.

Table 1

Parameter	Value (initial if variable)
stability of layer 1	0
Stability of layer 2	2×10^{-4} m^{-1}
Stability of layer 3	1×10^{-3} m^{-1}
Height of cloud base	300 m
Height of hill, H	665 m
Half width at half height	2000 m and 10000m
Roughness length, z_o	0.02 m
Geostrophic wind, U_g	15 ms^{-1}
Temperature, T (at cloud base)	5°C
Rainfall rate (washout model)	1 mmh^{-1}
Sulphate concentration in seeder rain	20μM
Height of inversion	400 m
Vertical Depth of Feeder Cloud	800m
Thickness of inversion	400 m

Chemical Agent loading of aerosol entering cap cloud 1.5×10^{-6} gm^{-3}

Legends to Figures

Figure 1

Schematic diagram showing turbulent deposition to a point ' a ' on the hill. The atmosphere has been divided into three layers, the lowest of which contains the cap cloud. — — represents the outer boundary of the region whose droplets may be deposited at ' a '. – – – represents the average path to ' a '. Axes in km.

Figure 2a

Cloud water turbulent deposition rates, D, for short hill case.

Curve a Standard conditions (see table 2)

Curve b Geostrophic windspeed doubled to 30ms^{-1}

Curve c Cloud raised to 500m

Curve d Chemical agent loading increased to 5 μgm^{-3} (same as curve a)

Curve e Neutral atmosphere

Curve g Forested hill. z_o=0.5m.

(curve f not shown, same as curves a and d)

Rates are in mmh^{-1}. Xaxis in km. Dashed line indicates extent of cloud when cloud base is 500m.

52

Figure 2b

Sulphate turbulent deposition rates , S, for short hill case.

Curve a Standard conditions (see table 2)

Curve b Geostrophic windspeed doubled to 30ms^{-1}

Curve c Cloud raised to 500m

Curve d Chemical Agent loading increased to 5 μgm^{-3}

Curve e Neutral atmosphere

Curve g Forested hill. z_o=0.5m.

Rates are in mgm^{-2}. X axis in km from centre of hill. Dashed line indicates extent of cloud when cloud base is 500m.

Figure 3

Deposition rate of chemical agent, S, to the hill surface for three different atmospheric conditions.

curve ' a ' is for a typical supercritical flow using the input shown in table 2.

curve ' b ' is an example of a sub-critical flow pattern (μ_2=1.5x10^{-3}, μ_3=1.5x10^{-3} m^{-1} height of layer 2 is 1200m and thickness 300m).

curve ' c ' has 0 stability in all 3 layers. X axis in km from centre of hill. Y axis is deposition rate in $mgm^{-2}h^{-1}$

51

Figure 4a

Cloud water turbulent deposition rates, D, for long hill case.

Curve a Standard conditions L=10km(see table 2)

Curve b Geostrophic windspeed doubled to 30ms $^{-1}$

Curve c Cloud raised to 500m

Curve e Neutral atmosphere

Curve g Forested hill. z_o=0.5m.

Rates are in mmh^{-1}. X axis in km. Dashed line indicates extent of cloud when cloud base is 500m.

Figure 4b

Chemical Agent turbulent deposition rates, s, for long hill case.

Curve a Standard conditions (see table 2)

Curve b Geostrophic windspeed doubled to 30ms^{-1}

Curve c Cloud raised to 500m

Curve d omitted for clarity (curve offscale)

Curve e Neutral atmosphere

Curve g Forested hill. z_o=0.5m.

Curve g' Forested hill. z_o=0.5m. No droplet depletion.

Rates are in mgm^{-2}. X axis in km from centre of hill. Dashed line indicates extent of cloud when cloud base is 500m.

52

Figure 5a.

Precipitation rates, P, for a 2km hill.

Curve a : standard (dashed line see table 2)

b : potential flow

c : 5 ms-1 wind

d : 400m thick cap cloud

e : 30 ms-1 wind

f : 5 mm h-1 precipitation rate (x a scaling factor of 0.1 , dotted line)

Rates are in $mmh^{-1}m^{-2}$. X axis in km from hill centre.

Figure 5b

Precipitation rates, P, for 10km hill

Curve a : standard (dashed line see table 2)

b : potential flow

c : 400m thick cap cloud

d : 30 ms-1 wind

e : 5 mm h-1 precipitation rate(x a scaling factor of 0.1 , dotted line)

Rates are in $mmh^{-1}m^{-2}$. X axis in km from hill centre.

Figure 6

Chemical Agent deposition rates, S, by seeder-feeder mechanism for short hill. Physical parameters are varied.

Curve a : standard conditions (see table 2)

Curve b : Potential flow, neutral atmosphere.

Curve c : 30 ms $^{-1}$ geostrophic wind

Curve d : 400 m cloud thickness

Curve e : 5 mmh^{-1} seeder precipitation rate (x a scaling factor of 0.5)

Rates are in mgh^{-1}m^{-2}. X axis in km from hill centre.

Figure 7

Chemical agent deposition, S, rates by seeder-feeder mechanism for long hill. Physical parameters are varied.

Curve a : standard conditions (see table 2)

Curve b : Potential flow, neutral atmosphere.

Curve c : 30 ms^{-1} geostrophic wind

Curve d : 400 m cloud thickness

curve e : 5 mmh^{-1} seeder precipitation rate (x 0.5)

Rates are in mgh^{-1}m^{-2}. X axis in km from hill centre.

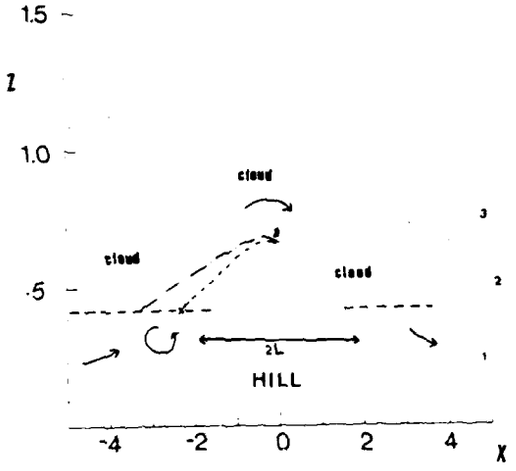
1.5
I
1.0
.5
cloud
cloud
cloud
3
2
1
2L
HILL
-4
-2
0
2
4
X

Figure 2a

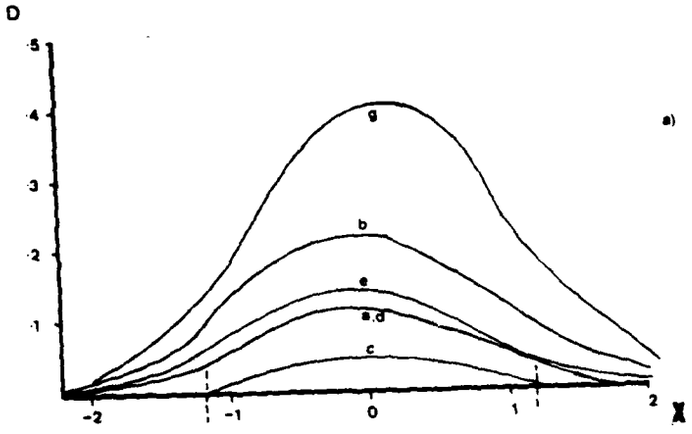
D
.5
.4
.3
.2
.1
g
b
e
a,d
c
a)
-2
-1
0
1
2
X

Figure 2b

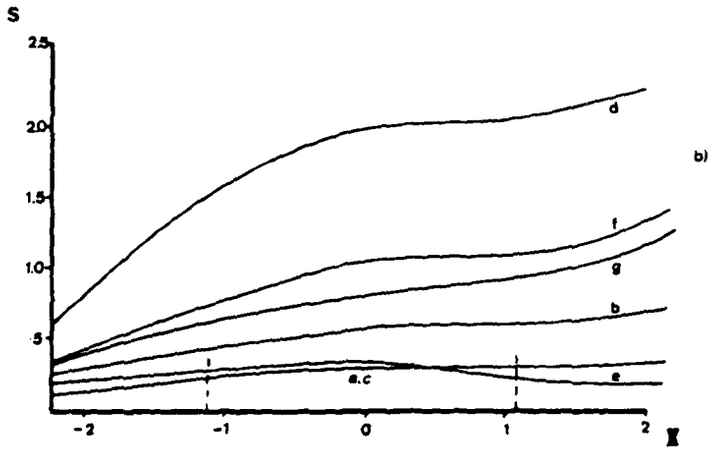

Figure 3

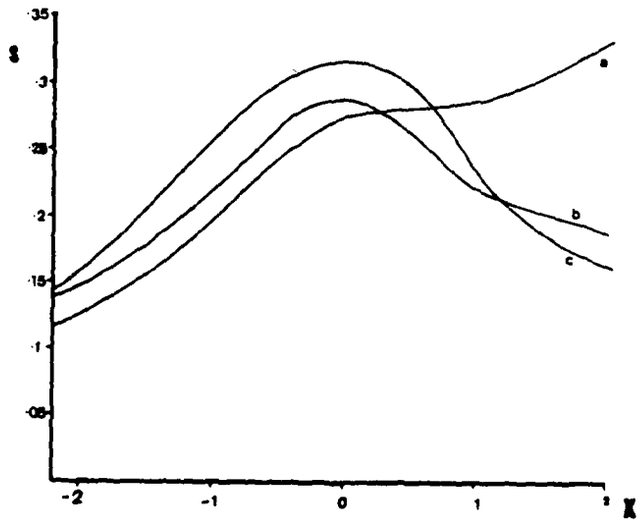

Figure 4a

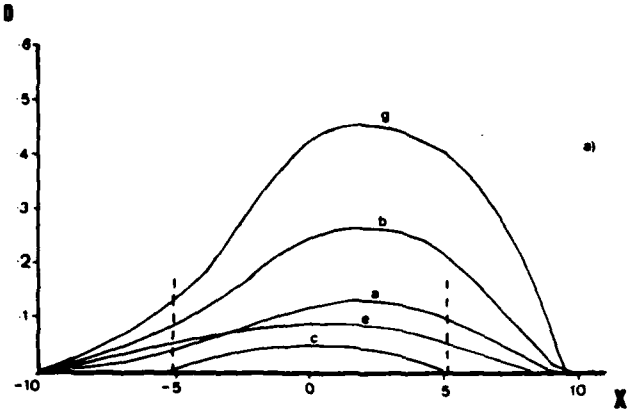

Figure 4b

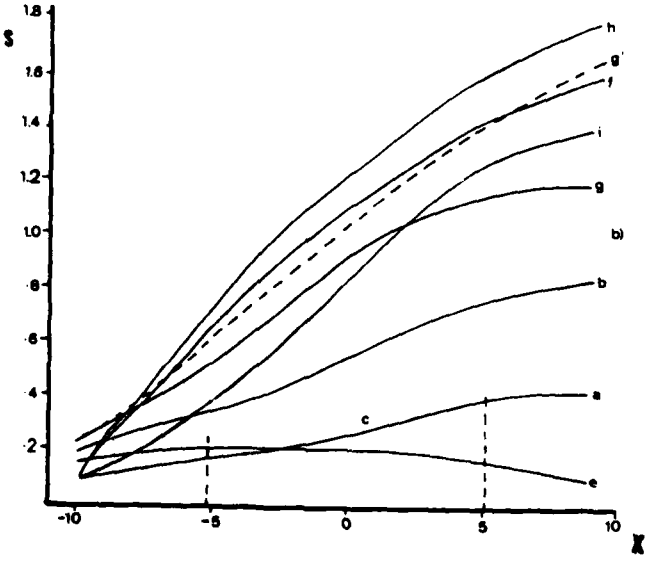

Figure 5a

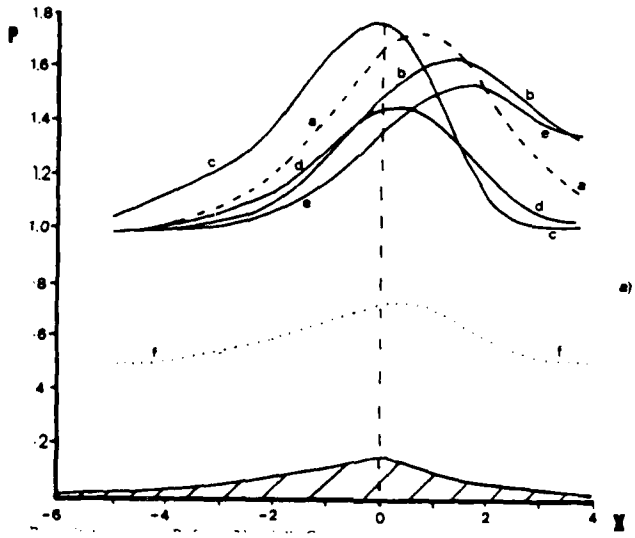

Figure 5b

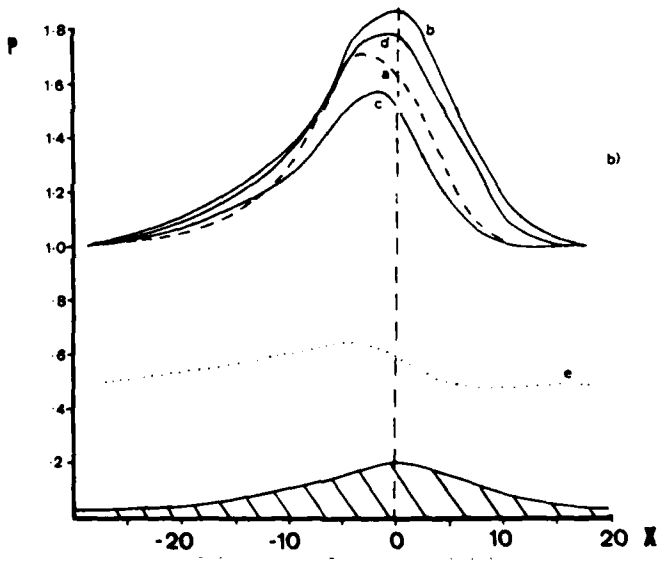

Figure 6

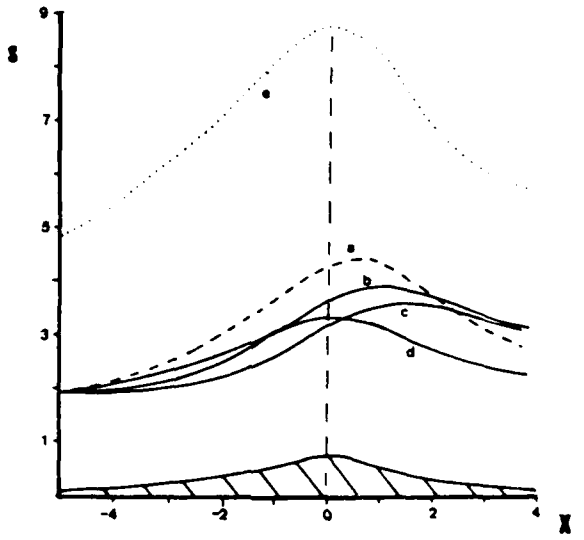

Figure 7

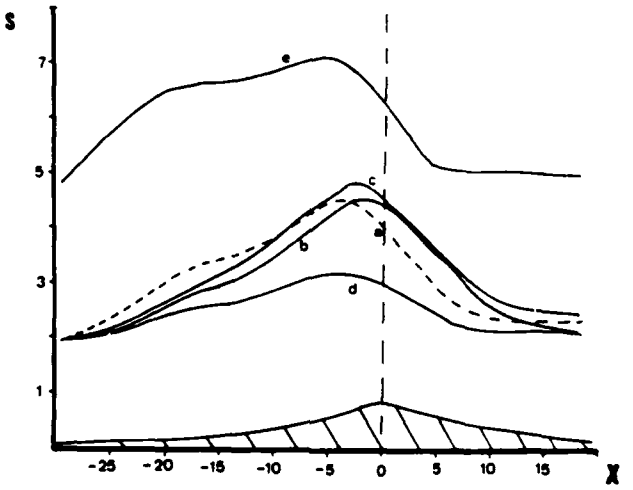

Sect 5.4

Dry Deposition Experiment: 26 May 1987

Introduction

This experiment formed part of the wider scale investigations into the dry deposition of particles and atmospheric pollutants carried out by the UMIST Atmospheric Physics Research Group.

The data acquisition was carried out at the Research Group's field station at Great Dun Fell (GDF) in Cumbria, on May 26th 1987. The primary aim was to study the rates of deposition of aerosol particles using the eddy correlation technique.

Dry Deposition and Eddy Correlation

Dry deposition is the removal of particles or gases from the atmosphere through the delivery of mass to the surface by non-precipitation atmospheric processes, and the subsequent chemical reaction with, or physical attachment to, vegetation, soil, or the built environment (Dolske, Gatz 1985).

Eddy correlation is the measurement of the net turbulent flux at the height of the sensing equipment. It is assumed that the sampling takes place within the surface boundary layer, as the theory requires that the flux divergence between the surface and the sensors is small.

The particle flux is given by:

$$\text{particle flux} = \overline{w'N'} = \overline{wN} - \bar{w}\,\bar{N}$$

where w = vertical wind speed, and N = particle concentration. The overbar denotes the mean value over a period of time, and ' indicates the variable component of the quantity.

However, it is usual to assume that $\bar{w} = 0$. This is not usually the case in practice, often due to misalignment of the vertical anemometer sensor. It is therefore necessary to mathematically correct for this when processing the data. We can realign all our data so that $\bar{w}$ and $\bar{v}$ are both zero (v is the transverse wind speed).

Neumann and Hartog (1985)use the following correction for the vertical particle flux:

$$\overline{w'N'} = (\overline{wN} - \bar{w}\,\bar{N})\cos\theta - (\overline{uN} - \bar{u}\,\bar{N})\cos\theta\sin\alpha - (\overline{vN} - \bar{v}\,\bar{N})\cos\theta\sin\alpha$$

where $\theta = \arctan\left|\frac{w}{|(u^2 + v^2)^{1/2}|}\right|$

and $\alpha = \arctan\left|\frac{v}{u}\right|$

and u = longitudinal wind speed

The deposition velocity is now given by:

$$v_d = \frac{\overline{w'N'}}{\bar{N}}$$

The values of v_d for aerosol particles are generally very small and it is therefore all the more important to de'ermine the level of error we have in our calculations. The following treatment of errors is

suggested by Katen and Hubbe (1985). The variance of the covariance of w' and N' is given by:

$$\sigma^2_{w'N'} = \overline{[(w')^2(N')^2]} - (\overline{w'N'})^2$$

The first term on the right hand side is the expectation value of $(w')^2$ and $(N')^2$. The second term is the square of the covariance. The standard error of an individual measurement of $\overline{w'N'}$ is given by:

$$\epsilon(w'N') = \frac{\sigma_{w'N'}}{n^{1/2}}$$

where n is the number of observations used in calculating the covariance. The standard error of the deposition velocity is then given by:

$$\epsilon(vd) = \frac{\sigma_{w'N'}}{\bar{N}\, n^{1/2}}$$

$\bar{N}$ is the average particle concentration during the sampling period and is assumed to be nearly constant.

Our data also allowed us to calculate values of the Monin-Obukhov length L, the heat flux, the friction velocity u_*, the stability parameter z/L and the roughness length z_o.

The Monin-Obukhov length is given by (Mason and King, 1984):

$$L = \frac{u_*^3 \bar{T}}{kg\overline{w'T'}}$$

where T is the absolute temperature, k is the von Karmann constant (= 0.4), and g is the gravitational acceleration (= 9.8kgms^{-2}). $\overline{w'T'}$ is the covariance of the vertical wind speed and the temperature and is given by:

$$\overline{w'T'} = \overline{wT} - \bar{w}\,\bar{T} = \frac{\text{heat flux}}{\rho C_p}$$

ρ is the air density, Cp is the specific heat of air at constant pressure. This quantity also has to be rotationally corrected into the mean wind direction.

The friction velocity u_* is given by:

$$u_*^2 = -\overline{u'w'}$$

The stability parameter is given by:

$$\frac{z}{L}$$

where z is the height at which sampling takes place.

The roughness length z_o is given by:

$$z_o = \frac{z}{\exp\left|\frac{ku(z)}{u_*} + \alpha\right|}$$

for $\frac{z}{L} < 0$: $\alpha = 2\ln\left|\frac{1 + x}{2}\right| + \ln\left|\frac{1 + x2}{2}\right| - 2\arctan x + \frac{\pi}{2}$

$$x = \left|1 - \frac{15z}{L}\right|^{\frac{1}{4}}$$

for $\frac{z}{L} > 0$: $\alpha = -4.7\frac{z}{L}$

The Experimental Set-Up

An Active Scattering Aerosol Spectrometer Probe (ASASP) model 300A, manufactured by Particle Measurement Systems (PMS), was used to measure particle concentrations. The ASASP allows particles in four different size ranges to be observed. The range chosen for this experiment was 0.4μm - 1.0μm diameter. This range is sub-divided into 15 categories, each of 0.04μm width. The ASASP was sampled at 4Hz.

The wind velocity was measured with a Kaijo-Denki USAT 310 sonic anemometer. This anemometer provides wind speeds in three mutually

25

perpendicular directions i.e. u,v and w. The anemometer also provides temperature data. The sonic anemometer was sampled at 40Hz.

The anemometer and ASASP were mounted on separate tripods. However, eddy correlation theory requires that the wind velocity sensor be as close to the particle sensor as possible. This was attempted by interlocking the legs of the tripod. The centre of the anemometer was 2.44m above the ground, 0.45m to the side of, 0.40m in front of, and 0.36m above the inlet of the ASASP (total distance from inlet is 0.70m). (A similar set-up is shown in Plate 1.)

The data from the sonic anemometer and the ASASP were logged by a NASCOM data acquisition system, and then transferred to magnetic tape. The data were processed using an IBM-compatible Tandon computer, using a specifically developed PASCAL program to compute the rotational corrections and covariances, and finally the values of particle fluxes and deposition velocities. (The anemometer data had first to be averaged up to 4 Hz.) These last two quantities were calculated both for each individual size category, and also as bulk quantities for the whole size range.

It would have been desirable to have an extensive uniform upwind fetch. Normally at GDF data acquisition takes place in south-westerly airflows, the direction in which the terrain is considered to be reasonably uniform. (This direction is also, conveniently, perpendicular to the axis of the ridge of which GDF forms a part. This is of particular importance when modelling the airflow over the ridge.) During the experiment the wind direction was easterly. However it is known that for the purposes of eddy correlation this wind direction is acceptable.

Results and Discussion

The measurements were initially made in two runs: 1642Z-1753Z and 1755Z-2102Z. On processing, the data were split into four runs, each of an hour duration: 1642Z-1742Z, 1755Z-1855Z, 1856Z-1956Z and 1957Z-2057Z. These times correspond to the transition between late afternoon and early evening (including sunset).

The effect of this is clearly shown by the presence of clear trends in the data (see table of results). The heat flux changes from around $100Wm^{-2}$ upwards during the first run to $20Wm^{-2}$ downwards during the final run. The stability changes from the unstable value of -0.046 in the first run to neutral/stable values in the other three runs.

z_o changes significantly during the period of the experiment. Although the stability changes may have had a small effect, the main cause of the change is thought to have been a change in wind direction.

The particle fluxes for individual sizes vary, often dramatically, from category to category. It was decided that it was therefore desirable to calculate the bulk fluxes and deposition velocities for the whole size range. The bulk flux of particles changes from around 40 $particlescc^{-1}s^{-1}$ downwards in the first run to 100 $particlescc^{-1}s^{-1}$ upwards in the final run. This trend is mirrored by the bulk deposition velocity which changes from $0.07cms^{-1}$ downwards in the first run to $0.17cms^{-1}$ upwards in the final run.

This accumulation of data trends tends to suggest that the transition from an afternoon of 11°C to a cool evening of 7°C has had a marked effect on the dry deposition of the aerosol particles under observation. We should therefore be very wary of drawing any solid

conclusions from our results. The clearest indications that we should not place our total trust in the results are the error calculations which suggest an error in the results of up to an order of magnitude.

Some of this error is most likely to have been caused by the unsatisfactory positioning of the sonic anemometer and the ASASP in relation to each other. It was noted earlier that eddy correlation theory requires that these pieces of equipment should be as close together as possible, ideally sampling at the same place. However, because the ASASP was only being sampled at 4Hz, this cause of error is unlikely to have been the major component of the calculated uncertainty. Having said this, it would still be desirable in the future to have a sample tube leading from the centre of the sonic anemometer to the ASASP inlet. This would, of course introduce a time delay between the ASASP and the anemometer, but this can be removed when processing the data.

The major cause of error is thought to have been the low sample volume of the ASASP, and doubts have been raised as to the suitability of the ASASP to eddy correlation studies. It's response time is slow compared with other particle measuring systems (such as the ASASX, also manufactured by PMS), and the sonic anemometer. The ASASP is more suited to measuring dry deposition using the gradient technique.

To be able to draw any conclusions on the dry deposition of aerosol particles would require further experimentation. In particular, periods of more constant conditions would be needed, and comparison between several days of data would be useful.

66

References

Dolske D.A. and Gatz D.F. *A field intercomparison of methods for the measurement of particle and gas dry deposition.* Jnl. of Geophs. Res., vol 90 no.D1, pp 2076-2084, Feb. 1985.

Katen P.C. and Hubbe J.M. *An evaluation of optical particle counter measurements of the dry deposition of atmospheric aerosol particles.* Jnl. of Geophs. Res., vol 90 no.D1, pp 2145-2160, Feb 1985.

Mason P.J. and King J.C. *Atmospheric flow over a succession of nearly two dimensional ridges and valleys.* Q. Jnl. of R. Met. Soc., vol 110 no.466, pp 821-846, Oct. 1984.

Neumann H.H. and den Hartog G. *Eddy correlation measurements of atmospheric fluxes of ozone, sulphur and particulates during the Champaign Intercomparison Study.* Jnl. of Geophs. Res., vol 90 no.D1, pp 2097-2110, Feb. 1985.

Dry Deposition Experiment at 26/52BZ.
Each flux is given as a 20 minute average. Positive indicates downwards.

TIME	V	U	W	T	SONIC DATA						ASASF DATA								
					CH1	CH2	CH3	CH4	CH5	CH6	CH7	CH8	CH9	CH10	CH11	CH12	CH13	CH14	CH15
1734:25	0.74	5.61	0.33	11.34	80.4	58.0	51.6	41.6	47.2	39.0	35.2	33.8	31.7	28.5	24.9	22.5	19.0	18.1	16.9
Flux (Particles/cm^2/s)					3.2	4.3	2.5	2.7	20.0	1.2	12.4	11.7	3.3	-1.0	7.7	4.5	1.6	-3.5	6.9
Flux (corrected for rotation)					7.5	4.0	4.1	2.4	17.0	4.5	10.6	9.1	2.6	-0.2	6.0	4.6	2.7	-1.9	9.3
Deposition Velocity (cm/s)					0.09	0.07	-0.08	0.05	0.40	-0.11	0.30	0.27	0.08	-0.01	0.24	0.21	0.14	-0.11	0.55

Roll Flux: 57.9 particles/cm^2/s u*: 0.39 m/s Z/L: 0.046
Bulk Deposition Velocity: 0.07 cm/s Zo: 6.4 mm
Monin Obukhov Length: 55.44 m Heat Flux: 100.26 W/m^2

TIME	V	U	W	T	SONIC DATA						ASASF DATA								
					CH1	CH2	CH3	CH4	CH5	CH6	CH7	CH8	CH9	CH10	CH11	CH12	CH13	CH14	CH15
1835:40	1.38	5.84	0.34	9.52	98.8	64.9	54.1	45.0	42.9	40.9	37.0	36.2	33.5	31.5	27.1	25.1	21.5	20.5	20.0
Flux (Particles/cm^2/s)					33.2	7.6	3.6	31.7	4.4	18.5	-1.5	11.3	-2.4	8.8	2.8	6.3	5.5	5.5	7.0
Flux (corrected for rotation)					22.7	7.3	3.7	11.5	2.9	19.0	-4.1	11.9	5.2	9.6	2.8	5.2	5.6	4.6	7.6
Deposition Velocity (cm/s)					0.24	0.11	0.02	0.26	0.07	0.46	-0.11	0.33	0.10	0.31	0.10	0.21	0.26	0.22	0.38

Roll Flux: 41.5 particles/cm^2/s u*: 0.36 m/s Z/L: 0.014
Bulk Deposition Velocity: 0.07 cm/s Zo: 2.6 mm
Monin Obukhov Length: 174.18 m Heat Flux: 33.43 W/m^2

TIME	V	U	W	T	SONIC DATA						ASASF DATA								
					CH1	CH2	CH3	CH4	CH5	CH6	CH7	CH8	CH9	CH10	CH11	CH12	CH13	CH14	CH15
1935:44	1.70	5.81	0.35	7.02	111.0	74.8	58.6	45.6	43.5	40.7	37.5	37.0	34.6	33.2	28.9	27.4	23.3	22.6	21.0
Flux (Particles/cm^2/s)					2.9	10.5	-0.7	30.4	14.5	6.4	-4.6	7.4	4.0	6.9	-6.0	6.2	8.3	4.9	7.2
Flux (corrected for rotation)					24.7	4.4	-5.2	7.1	13.1	4.5	7.0	6.1	1.8	4.5	-8.2	3.7	7.5	4.2	6.4
Deposition Velocity (cm/s)					0.20	0.06	-0.09	0.15	0.30	0.11	-0.19	0.16	0.05	0.14	-0.28	0.13	0.32	0.19	0.29

Roll Flux: 18.1 particles/cm^2/s u*: 0.33 m/s Z/L: 0.005
Bulk Deposition Velocity: 0.03 cm/s Zo: 0.9 mm
Monin Obukhov Length: 480.23 m Heat Flux: 6.25 W/m^2

TIME	V	U	W	T	SONIC DATA						ASASF DATA								
					CH1	CH2	CH3	CH4	CH5	CH6	CH7	CH8	CH9	CH10	CH11	CH12	CH13	CH14	CH15
2035:33	1.01	5.42	0.31	7.13	111.4	74.8	59.2	46.2	42.9	39.3	35.2	33.4	30.5	28.0	25.7	21.6	18.6	17.5	16.6
Flux (Particles/cm^2/s)					25.2	7.6	0.1	2.0	-12.7	7.7	1.8	4.1	12.9	-4.2	5.1	1.5	8.9	5.7	2.4
Flux (corrected for rotation)					41.0	2.7	5.0	6.9	18.2	1.8	-5.6	-3.5	5.2	-12.6	2.2	-5.7	2.0	-0.9	-5.2
Deposition Velocity (cm/s)					-0.14	-0.04	0.08	0.15	-0.42	0.05	-0.16	-0.11	0.17	0.45	-0.09	-0.27	0.11	-0.05	-0.32

Roll Flux: 100.7 particles/cm^2/s u*: 0.28 m/s Z/L: 0.028
Bulk Deposition Velocity: 0.17 cm/s Zo: 0.4 mm
Monin Obukhov Length: 86.94 m Heat Flux: 22.21 W/m^2

16:42:22 to 17:42:25 on 25 May 1987
Error in bulk flux is 384.37
Error in bulk deposition velocity is 0.705
17:55: 6 to 18:55:40 on 25 May 1987
Error in bulk flux is 306.96
Error in bulk deposition velocity is 0.513
18:55:45 to 19:56:44 on 25 May 1987
Error in bulk flux is 362.95
Error in bulk deposition velocity is 0.557
19:56:49 to 20:57:33 on 25 May 1987
Error in bulk flux is 355.85
Error in bulk deposition velocity is 0.583

PLATE 1 The Apparatus used for the aerosol deposition measurements.

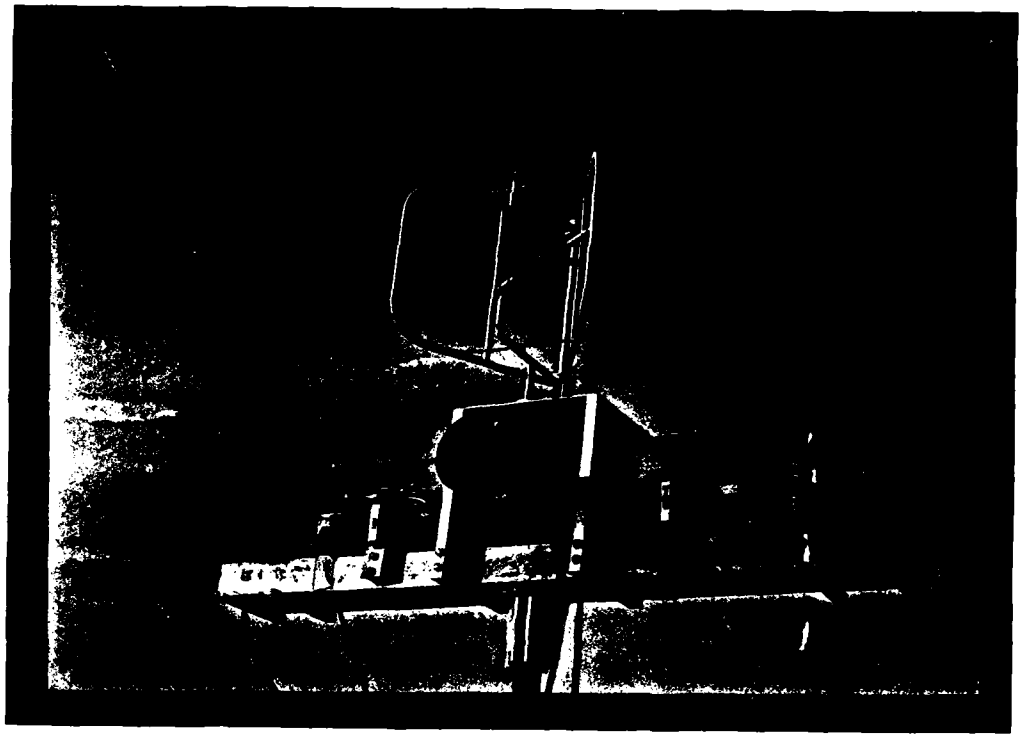

SECTION 5

MEASUREMENTS OF AEROSOL SIZE DISTRIBUTIONS AT GREAT DUN FELL

a. Intercomparison of Probes

Prior to this experiment the UMIST Knollenberg ASASP was compared in detail with the University of Galway Knollenberg ASAS-X probe. These experiments were performed in the laboratory at UMIST and involved intercomparisons using the background aerosol, latex spheres of known size and an ammonium sulphate aerosol distribution generated from a nebuliser. The results of this intercomparison are summarised in Table 1 and will be used to compare the results obtained by the University of Galway with those obtained by UMIST.

b. The Field Measurements

Measurements were made simultaneously by the two institutions during the period 18-20 April 1988. The air trajectories passed close to both sites on 20 April when the transit time between W. Ireland and Great Dun Fell was about 10 hours. The UMIST ASASP was located at the site of our mobile laboratory which was located on the SW face of Great Dun Fell approximately 150m below the hill summit of 847m. The ASASP was mounted 1.0m above the ground and pointed into wind. Measurements of wind speed, wind direction wet and dry bulb temperature were made. The results obtained are shown in table 2. The next step in analysing this data will be to compare the results with those obtained by the University of Galway.

Section 5

Data from 19th April 1988.

All counts are 15 minute averages, and are given in particles/cc/sec. The data are corrected for the sample volume difference between the ASAS-X and ASAS-P.

19/4/88

Record nos. 970 - 984
9:45:22 - 10: 0:22

ch1	ch2	ch3	ch4	ch5	ch6	ch7	ch8	ch9	ch10	ch11	ch12	ch13	ch14	ch15
14	11	8	6	5	4	3	2	2	2	2	2	1	1	1

** m/s	dd deg	Tw deg C	Td deg C	humidity
5.0	215	8.8	8.6	100.00%

Record nos. 985 - 999
10: 0:24 - 10:15:35

ch1	ch2	ch3	ch4	ch5	ch6	ch7	ch8	ch9	ch10	ch11	ch12	ch13	ch14	ch15
12	11	9	8	7	6	6	5	4	4	4	4	4	3	3

** m/s	dd deg	Tw deg C	Td deg C	humidity
4.8	217	8.8	8.7	100.00%

Record nos. 1000 - 1014
10:15:26 - 10:30:26

ch1	ch2	ch3	ch4	ch5	ch6	ch7	ch8	ch9	ch10	ch11	ch12	ch13	ch14	ch15
11	9	6	6	5	4	4	3	3	3	3	3	3	2	2

** m/s	dd deg	Tw deg C	Td deg C	humidity
5.2	218	8.8	8.7	100.00%

Record nos. 1015 - 1029
10:30:27 - 10:45:27

ch1	ch2	ch3	ch4	ch5	ch6	ch7	ch8	ch9	ch10	ch11	ch12	ch13	ch14	ch15
14	11	8	7	7	6	5	4	3	3	3	3	3	2	2

** m/s	dd deg	Tw deg C	Td deg C	humidity
5.0	211	8.8	8.7	100.00%

Record nos. 1030 - 1044
10:45:28 - 11: 0:28

ch1	ch2	ch3	ch4	ch5	ch6	ch7	ch8	ch9	ch10	ch11	ch12	ch13	ch14	ch15
12	10	8	7	6	4	3	3	2	2	2	2	1	1	1

** m/s	dd deg	Tw deg C	Td deg C	humidity
4.8	207	9.0	9.0	99.22%

Record nos. 1045 - 1059
11: 0:29 - 11:15:29

ch1	ch2	ch3	ch4	ch5	ch6	ch7	ch8	ch9	ch10	ch11	ch12	ch13	ch14	ch15
27	22	20	17	13	9	8	1	1	1	1	1	1	1	1

** m/s	dd deg	Tw deg C	Td deg C	humidity
5.2	215	9.9	10.1	97.52%

Record nos. 1060 - 1074
11:15:30 - 11:30:31

ch1	ch2	ch3	ch4	ch5	ch6	ch7	ch8	ch9	ch10	ch11	ch12	ch13	ch14	ch15
21	18	13	9	7	6	5	2	1	1	1	1	1	1	1

** m/s	dd deg	Tw deg C	Td deg C	humidity
5.0	216	10.1	10.4	96.77%

Record nos. 1075 - 1089
11:30:12 - 11:45:12

ch1	ch2	ch3	ch4	ch5	ch6	ch7	ch8	ch9	ch10	ch11	ch12	ch13	ch14	ch15
13	6	4	3	2	1	1	1	1	1	0	0	0	0	0

** m/s	dd deg	Tw deg C	Td deg C	humidity
6.0	221	9.8	10.2	94.45%

Record nos. 1090 - 1104
11:45:12 - 12: 0:12

ch1	ch2	ch3	ch4	ch5	ch6	ch7	ch8	ch9	ch10	ch11	ch12	ch13	ch14	ch15
8	4	3	2	1	1	1	0	0	0	0	0	0	0	0

** m/s	dd deg	Tw deg C	Td deg C	humidity
6.1	226	8.9	9.4	94.07%

Record nos. 1105 - 1119
12: 0:24 - 12:15:24

ch1	ch2	ch3	ch4	ch5	ch6	ch7	ch8	ch9	ch10	ch11	ch12	ch13	ch14	ch15
12	7	4	4	2	2	2	1	0	0	0	0	0	0	0

** m/s	dd deg	Tw deg C	Td deg C	humidity
5.2	225	9.2	9.8	90.03%

Record nos. 1120 - 1134
12:15:36 - 12:30:36

ch1	ch2	ch3	ch4	ch5	ch6	ch7	ch8	ch9	ch10	ch11	ch12	ch13	ch14	ch15
8	5	3	2	1	1	1	1	0	0	0	0	0	0	0

** m/s	dd deg	Tw deg C	Td deg C	humidity
5.4	222	9.9	10.7	89.74%

Record nos. 1135 - 1149
12:30:36 - 12:45:37

ch1	ch2	ch3	ch4	ch5	ch6	ch7	ch8	ch9	ch10	ch11	ch12	ch13	ch14	ch15
8	7	4	3	1	1	1	1	1	1	1	1	1	1	1

** m/s	dd deg	Tw deg C	Td deg C	humidity
6.2	227	10.1	11.2	86.79%

Record nos. 1150 - 1164
12:45:38 - 13: 0:38

ch1	ch2	ch3	ch4	ch5	ch6	ch7	ch8	ch9	ch10	ch11	ch12	ch13	ch14	ch15
9	4	3	2	2	1	1	1	1	1	1	1	1	1	1

** m/s	dd deg	Tw deg C	Td deg C	humidity
5.8	227	10.0	11.2	86.47%

Record nos. 1165 - 1179
13: 0:39 - 13:15:39

ch1	ch2	ch3	ch4	ch5	ch6	ch7	ch8	ch9	ch10	ch11	ch12	ch13	ch14	ch15
4	2	1	1	1	0	0	0	0	0	0	0	0	0	0

** m/s	dd deg	Tw deg C	Td deg C	humidity
5.9	222	10.1	11.2	86.39%

Record nos. 1180 - 1194
17:15:40 - 17:20:40

ch1	ch2	ch3	ch4	ch5	ch6	ch7	ch8	ch9	ch10	ch11	ch12	ch13	ch14	ch15
4	2	1	1	0	1	0	0	0	0	0	1	0	0	1

** m/s	dd deg	Tw deg C	Td deg C	humidity
6.0	274	9.7	11.1	82.60%

Record nos. 1195 - 1209
17:20:41 - 17:45:41

ch1	ch2	ch3	ch4	ch5	ch6	ch7	ch8	ch9	ch10	ch11	ch12	ch13	ch14	ch15
2	1	1	1	0	0	0	0	0	0	0	0	0	0	0

** m/s	dd deg	Tw deg C	Td deg C	humidity
5.7	272	9.7	11.1	80.45%

Record nos. 1210 - 1224
17:45:42 - 18:10:42

ch1	ch2	ch3	ch4	ch5	ch6	ch7	ch8	ch9	ch10	ch11	ch12	ch13	ch14	ch15
2	1	1	1	0	0	0	0	0	0	0	0	0	0	0

** m/s	dd deg	Tw deg C	Td deg C	humidity
5.5	274	10.2	12.1	77.57%

Record nos. 1225 - 1239
18:10:43 - 18:15:44

ch1	ch2	ch3	ch4	ch5	ch6	ch7	ch8	ch9	ch10	ch11	ch12	ch13	ch14	ch15
2	1	1	0	0	0	0	0	0	0	0	0	0	0	0

** m/s	dd deg	Tw deg C	Td deg C	humidity
5.1	278	10.4	12.5	75.01%

Record nos. 1240 - 1254
18:15:45 - 18:20:45

ch1	ch2	ch3	ch4	ch5	ch6	ch7	ch8	ch9	ch10	ch11	ch12	ch13	ch14	ch15
2	1	1	0	0	0	0	0	0	0	0	0	0	0	0

** m/s	dd deg	Tw deg C	Td deg C	humidity
4.2	246	9.8	12.0	74.20%

Record nos. 1255 - 1269
18:20:46 - 18:45:46

ch1	ch2	ch3	ch4	ch5	ch6	ch7	ch8	ch9	ch10	ch11	ch12	ch13	ch14	ch15
2	1	1	0	0	0	0	0	0	0	0	0	0	0	0

** m/s	dd deg	Tw deg C	Td deg C	humidity
4.6	257	9.7	11.9	75.20%

Record nos. 1270 - 1284
18:45:47 - 19:10:47

ch1	ch2	ch3	ch4	ch5	ch6	ch7	ch8	ch9	ch10	ch11	ch12	ch13	ch14	ch15
2	1	1	1	1	0	0	0	0	0	0	0	0	0	0

** m/s	dd deg	Tw deg C	Td deg C	humidity
5.7	275	9.2	11.3	79.30%

Record nos. 1285 - 1299
15: 0:49 - 15:15:49

ch1	ch2	ch3	ch4	ch5	ch6	ch7	ch8	ch9	ch10	ch11	ch12	ch13	ch14	ch15
2	1	1	1	0	0	0	0	0	0	0	0	0	0	1

** m/s	dd deg	Tw deg C	Td deg C	humidity
5.7	265	9.9	12.0	74.68%

Record nos. 1300 - 1314
15:15:50 - 15:30:50

ch1	ch2	ch3	ch4	ch5	ch6	ch7	ch8	ch9	ch10	ch11	ch12	ch13	ch14	ch15
2	1	1	1	0	0	0	0	0	0	0	0	0	0	0

** m/s	dd deg	Tw deg C	Td deg C	humidity
4.7	256	10.0	12.3	73.07%

Record nos. 1315 - 1329
15:30:51 - 15:45:51

ch1	ch2	ch3	ch4	ch5	ch6	ch7	ch8	ch9	ch10	ch11	ch12	ch13	ch14	ch15
2	1	1	1	0	0	0	0	0	0	0	0	0	0	0

** m/s	dd deg	Tw deg C	Td deg C	humidity
4.2	240	9.7	12.3	72.89%

Record nos. 1330 - 1344
15:45:52 - 16: 0:52

ch1	ch2	ch3	ch4	ch5	ch6	ch7	ch8	ch9	ch10	ch11	ch12	ch13	ch14	ch15
2	1	1	1	0	0	0	0	0	0	0	0	0	0	0

** m/s	dd deg	Tw deg C	Td deg C	humidity
4.4	244	9.4	11.5	74.71%

Record nos. 1345 - 1359
16: 0:53 - 16:15:54

ch1	ch2	ch3	ch4	ch5	ch6	ch7	ch8	ch9	ch10	ch11	ch12	ch13	ch14	ch15
4	2	1	1	1	0	0	0	0	0	0	0	0	0	0

** m/s	dd deg	Tw deg C	Td deg C	humidity
4.5	249	9.2	11.5	74.74%

Record nos. 1360 - 1374
16:15:55 - 16:30:55

ch1	ch2	ch3	ch4	ch5	ch6	ch7	ch8	ch9	ch10	ch11	ch12	ch13	ch14	ch15
10	5	4	3	2	2	1	0	0	0	0	0	0	0	1

** m/s	dd deg	Tw deg C	Td deg C	humidity
4.0	245	9.1	11.1	76.39%

Record nos. 1375 - 1389
16:30:56 - 16:45:56

ch1	ch2	ch3	ch4	ch5	ch6	ch7	ch8	ch9	ch10	ch11	ch12	ch13	ch14	ch15
5	2	2	1	1	0	0	0	0	0	0	0	0	0	0

** m/s	dd deg	Tw deg C	Td deg C	humidity
4.0	232	8.9	10.7	77.78%

Record nos. 1391 - 1404
16:45:57 - 17: 0:57

ch1	ch2	ch3	ch4	ch5	ch6	ch7	ch8	ch9	ch10	ch11	ch12	ch13	ch14	ch15
11	4	3	2	1	1	1	1	1	1	1	1	1	1	1

## m/s	dd deg	Tw deg C	Td deg C	humidity
4.5	22e	8.3	11.5	78.6%

Record nos. 1405 - 1419
17: 0:58 - 17:15:59

ch1	ch2	ch3	ch4	ch5	ch6	ch7	ch8	ch9	ch10	ch11	ch12	ch13	ch14	ch15
21	10	6	5	4	2	2	0	0	0	0	0	0	0	0

## m/s	dd deg	Tw deg C	Td deg C	humidity
4.6	225	8.7	10.3	89.23%

Record nos. 1420 - 1434
17:16: 0 - 17:31: 0

ch1	ch2	ch3	ch4	ch5	ch6	ch7	ch8	ch9	ch10	ch11	ch12	ch13	ch14	ch15
22	12	7	5	4	3	2	1	1	1	1	1	1	1	1

## m/s	dd deg	Tw deg C	Td deg C	humidity
4.7	219	9.1	11.1	80.29%

Record nos. 1435 - 1449
17:31: 1 - 17:46: 1

ch1	ch2	ch3	ch4	ch5	ch6	ch7	ch8	ch9	ch10	ch11	ch12	ch13	ch14	ch15
18	7	5	3	2	1	1	1	1	1	1	1	1	1	1

## m/s	dd deg	Tw deg C	Td deg C	humidity
3.4	219	9.2	11.1	82.47%

Record nos. 1450 - 1464
17:46: 2 - 18: 1: 2

ch1	ch2	ch3	ch4	ch5	ch6	ch7	ch8	ch9	ch10	ch11	ch12	ch13	ch14	ch15
14	7	5	3	2	2	1	1	1	1	1	1	1	1	1

## m/s	dd deg	Tw deg C	Td deg C	humidity
3.4	227	9.4	9.6	94.57%

Record nos. 1465 - 1479
18: 1: 3 - 18:16: 4

ch1	ch2	ch3	ch4	ch5	ch6	ch7	ch8	ch9	ch10	ch11	ch12	ch13	ch14	ch15
17	9	6	4	3	2	1	1	1	1	1	1	1	1	1

## m/s	dd deg	Tw deg C	Td deg C	humidity
3.4	210	8.2	9.4	86.99%

Record nos. 1480 - 1494
18:16: 5 - 18:31: 5

ch1	ch2	ch3	ch4	ch5	ch6	ch7	ch8	ch9	ch10	ch11	ch12	ch13	ch14	ch15
17	9	7	4	3	2	2	1	1	1	1	1	1	1	1

## m/s	dd deg	Tw deg C	Td deg C	humidity
3.5	257	8.2	9.1	87.68%

Record nos. 1496 - 1509
19:01:0 - 19:48:0

ch1	ch2	ch3	ch4	ch5	ch6	ch7	ch8	ch9	ch10	ch11	ch12	ch13	ch14	ch15
17	9	7	5	3	2	2	1	1	1	1	1	1	1	1

ff m/s	dd/deg	Tw deg C	Td deg C	humidity
7.5	255	7.8	5.6	89.12%

Record nos. 1511 - 1524
19:48:3 - 19:01:3

ch1	ch2	ch3	ch4	ch5	ch6	ch7	ch8	ch9	ch10	ch11	ch12	ch13	ch14	ch15
22	12	8	5	4	3	2	1	1	1	1	1	1	1	1

ff m/s	dd/deg	Tw deg C	Td deg C	humidity
2.5	290	7.7	7.4	92.17%

Record nos. 1526 - 1539
19:01:5 - 19:48:3

ch1	ch2	ch3	ch4	ch5	ch6	ch7	ch8	ch9	ch10	ch11	ch12	ch13	ch14	ch15
11	5	3	2	1	1	1	1							

ff m/s	dd deg	Tw deg C	Td deg C	humidity
1.5	297	6.6	6.1	93.17%

Record nos. 1541 - 1554
19:48:10 - 19:01:10

ch1	ch2	ch3	ch4	ch5	ch6	ch7	ch8	ch9	ch10	ch11	ch12	ch13	ch14	ch15
11	6	4	3	2	1	1	1							

ff m/s	dd deg	Tw deg C	Td deg C	humidity
1.5	299	6.1	5.5	94.74%

Record nos. 1556 - 1569
19:01:11 - 19:48:11

ch1	ch2	ch3	ch4	ch5	ch6	ch7	ch8	ch9	ch10	ch11	ch12	ch13	ch14	ch15
11	7	4	3	2	1	1	1	1						

ff m/s	dd deg	Tw deg C	Td deg C	humidity
1.5	329	5.9	5.4	94.19%

Record nos. 1571 - 1584
19:48:12 - 20:01:12

ch1	ch2	ch3	ch4	ch5	ch6	ch7	ch8	ch9	ch10	ch11	ch12	ch13	ch14	ch15
14	8	6	4	3	2	2	1	1	1	1	1	1	1	1

ff m/s	dd deg	Tw deg C	Td deg C	humidity
1.2	291	5.4	5.1	95.63%

Record nos. 1586 - 1599
20:01:13 - 20:48:13

ch1	ch2	ch3	ch4	ch5	ch6	ch7	ch8	ch9	ch10	ch11	ch12	ch13	ch14	ch15
2	1	1	1	1	1	1	1	1	1	1	1	1	1	1

ff m/s	dd deg	Tw deg C	Td deg C	humidity
1.5	288	5.3	4.1	94.82%

Record nos. 1600 - 1614
21:16:15 - 21:31:15

ch1	ch2	ch3	ch4	ch5	ch6	ch7	ch8	ch9	ch10	ch11	ch12	ch13	ch14	ch15
0	0	0	0	0	0	0	0	0	0	0	0	0	0	0

Ws m/s	Wd deg	Tw deg C	Td deg C	humidity
1.2	246	5.4	5.5	96.23%

Record nos. 1615 - 1629
21:31:15 - 21:46:15

ch1	ch2	ch3	ch4	ch5	ch6	ch7	ch8	ch9	ch10	ch11	ch12	ch13	ch14	ch15
0	0.18520	0	0	0	0	0	0	0	0	0	0	0	0	0

Ws m/s	Wd deg	Tw deg C	Td deg C	humidity
1.2	213	5.5	5.7	95.29%

Data from 20th April 1988.

All counts are 15 minute averages, and are given in paricles/cc/sec. The data are corrected for the sample volume difference between the ASAS-X and ASAS-P.

20/4/88

Record nos. 2690 - 2604
12:47:25 - 17: 2:25

ch1	ch2	ch3	ch4	ch5	ch6	ch7	ch8	ch9	ch10	ch11	ch12	ch13	ch14	ch15
11	5	3	2	2	2	1	1				0		1	

** m s	dd deg	Tw deg C	Td deg C	humidity
8.7	252	7.1	5.2	87.48%

Record nos. 2615 - 2619
17: 2:26 - 17:17:26

ch1	ch2	ch3	ch4	ch5	ch6	ch7	ch8	ch9	ch10	ch11	ch12	ch13	ch14	ch15
9	4	2	2	1	1	1	0	1	0	0	0	1	1	

** m s	dd deg	Tw deg C	Td deg C	humidity
7.5	254	6.4	4.4	86.86%

Record nos. 2620 - 2624
17:17:27 - 17:32:27

ch1	ch2	ch3	ch4	ch5	ch6	ch7	ch8	ch9	ch10	ch11	ch12	ch13	ch14	ch15
8	4	2	1	1	1	1	0	1	1	1	0	1	0	1

** m s	dd deg	Tw deg C	Td deg C	humidity
6.1	241	5.8	3.8	87.66%

Record nos. 2625 - 2629
17:32:28 - 17:47:28

ch1	ch2	ch3	ch4	ch5	ch6	ch7	ch8	ch9	ch10	ch11	ch12	ch13	ch14	ch15
17	9	5	3	2	2	1	1	1	1	1	1	1		

** m s	dd deg	Tw deg C	Td deg C	humidity
4.4	222	5.1	3.3	94.75%

Record nos. 2630 - 2634
17:47:29 - 18: 2:29

ch1	ch2	ch3	ch4	ch5	ch6	ch7	ch8	ch9	ch10	ch11	ch12	ch13	ch14	ch15
48	25	17	12	9	8	5	3	2	1	1	1	1	1	1

** m s	dd deg	Tw deg C	Td deg C	humidity
8.8	274	6.1	4.2	95.67%

Record nos. 2635 - 2639
18: 2:30 - 18:17:30

ch1	ch2	ch3	ch4	ch5	ch6	ch7	ch8	ch9	ch10	ch11	ch12	ch13	ch14	ch15
16	9	5	3	2	2	1	1	1	1	1	1	1	1	

** m s	dd deg	Tw deg C	Td deg C	humidity
8.0	278	5.8	3.7	97.57%

Record nos. 2640 - 2644
18:17:31 - 18:32:31

ch1	ch2	ch3	ch4	ch5	ch6	ch7	ch8	ch9	ch10	ch11	ch12	ch13	ch14	ch15
11	6	3	2	1	1	1	1	1	1	1	0	1	1	

** m s	dd deg	Tw deg C	Td deg C	humidity
7.4	264	5.7	3.7	96.13%

Record nos. 2695 - 2709
14:12:47 - 14:47:47

ch1	ch2	ch3	ch4	ch5	ch6	ch7	ch8	ch9	ch10	ch11	ch12	ch13	ch14	ch15
0	5	1	1	1	1	1	1							

** n/a	dd deg	Tw deg C	Td deg C	humidity
7.6	247	5.7	6.4	94.20%

Record nos. 2710 - 2724
14:47:44 - 15: 2:44

ch1	ch2	ch3	ch4	ch5	ch6	ch7	ch8	ch9	ch10	ch11	ch12	ch13	ch14	ch15
5	7	2	1	1	1	0	0	0	0	0	0	0	0	1

** n/a	dd deg	Tw deg C	Td deg C	humidity
8.7	252	5.7	6.7	93.12%

Record nos. 2725 - 2739
15: 2:45 - 15:17:45

ch1	ch2	ch3	ch4	ch5	ch6	ch7	ch8	ch9	ch10	ch11	ch12	ch13	ch14	ch15
5	7	2	1	1	1	1				0		0		1

** n/a	dd deg	Tw deg C	Td deg C	humidity
9.5	253	5.1	5.9	91.65%

Record nos. 2740 - 2754
15:17:45 - 15:32:47

ch1	ch2	ch3	ch4	ch5	ch6	ch7	ch8	ch9	ch10	ch11	ch12	ch13	ch14	ch15
5	7	2	1	1	1	1	1	1	1	1	0	1	0	1

** n/a	dd deg	Tw deg C	Td deg C	humidity
9.9	254	5.4	7.0	92.45%

Record nos. 2755 - 2769
15:32:46 - 15:47:48

ch1	ch2	ch3	ch4	ch5	ch6	ch7	ch8	ch9	ch10	ch11	ch12	ch13	ch14	ch15
0	4	2	2	1	1	1	1	1	1	1	0	1	0	1

** n/a	dd deg	Tw deg C	Td deg C	humidity
10.4	251	6.1	6.6	92.55%

Record nos. 2770 - 2784
15:47:49 - 16: 2:49

ch1	ch2	ch3	ch4	ch5	ch6	ch7	ch8	ch9	ch10	ch11	ch12	ch13	ch14	ch15
3	4	2	2	2	1	1	1	1	1	1	0	1	0	1

** n/a	dd deg	Tw deg C	Td deg C	humidity
10.1	252	6.6	7.0	94.05%

Record nos. 2785 - 2799
16: 2:51 - 16:17:50

ch1	ch2	ch3	ch4	ch5	ch6	ch7	ch8	ch9	ch10	ch11	ch12	ch13	ch14	ch15
3	4	2	2	1	1	1	1	1	1	1	0	1	0	1

** n/a	dd deg	Tw deg C	Td deg C	humidity
10.1	247	6.4	6.9	93.25%

Record nos. 2801 - 2814
18:17:51 - 18:22:51

ch1	ch2	ch3	ch4	ch5	ch6	ch7	ch8	ch9	ch10	ch11	ch12	ch13	ch14	ch15
3	2	2	1	1	1	1	1	1	1	1	0	1	1	1

** m/s	dd deg	Tw deg C	Td deg C	humidity
10.2	247	6.5	7.1	91.85%

Record nos. 2815 - 2829
18:22:52 - 18:47:52

ch1	ch2	ch3	ch4	ch5	ch6	ch7	ch8	ch9	ch10	ch11	ch12	ch13	ch14	ch15
40	22	17	12	10	8	7	1	1	1	1	0	1	1	1

** m/s	dd deg	Tw deg C	Td deg C	humidity
10.5	244	6.2	6.7	97.40%

Record nos. 2830 - 2844
18:47:57 - 17: 2:54

ch1	ch2	ch3	ch4	ch5	ch6	ch7	ch8	ch9	ch10	ch11	ch12	ch13	ch14	ch15
11	6	4	3	2	1	1	1	1	1	1	1	1	1	1

** m/s	dd deg	Tw deg C	Td deg C	humidity
9.4	237	6.0	6.2	96.61%

Record nos. 2845 - 2859
17: 2:55 - 17:17:55

ch1	ch2	ch3	ch4	ch5	ch6	ch7	ch8	ch9	ch10	ch11	ch12	ch13	ch14	ch15
45	26	15	14	11	11	7	1	1	1	1	1	1	1	1

** m/s	dd deg	Tw deg C	Td deg C	humidity
10.2	241	6.0	6.2	98.73%

Record nos. 2860 - 2874
17:17:56 - 17:32:56

ch1	ch2	ch3	ch4	ch5	ch6	ch7	ch8	ch9	ch10	ch11	ch12	ch13	ch14	ch15
30	14	8	5	3	3	2	2	1	1	1	1	1	1	1

** m/s	dd deg	Tw deg C	Td deg C	humidity
10.4	242	5.9	6.0	98.65%

Record nos. 2875 - 2889
17:32:57 - 17:47:57

ch1	ch2	ch3	ch4	ch5	ch6	ch7	ch8	ch9	ch10	ch11	ch12	ch13	ch14	ch15
92	47	23	22	19	15	12	2	1	1	1	1	1	1	1

** m/s	dd deg	Tw deg C	Td deg C	humidity
11.0	240	5.7	5.7	99.15%

Record nos. 2890 - 2904
17:47:58 - 18: 2:58

ch1	ch2	ch3	ch4	ch5	ch6	ch7	ch8	ch9	ch10	ch11	ch12	ch13	ch14	ch15
988	497	251	126	226	220	174	5	3	2	2	2	2	2	2

** m/s	dd deg	Tw deg C	Td deg C	humidity
10.1	241	5.5	5.4	100.00%

Record nos. 2905 - 2919
19: 1:59 - 19:13: 0

ch1	ch2	ch3	ch4	ch5	ch6	ch7	ch8	ch9	ch10	ch11	ch12	ch13	ch14	ch15
245	76	19	12	5	4	2	1	2	2	1	2	1	1	1

** m/s	dd deg	Tw deg C	Td deg C	humidity
9.9	240	5.4	5.1	100.00%

Record nos. 2920 - 2934
19:13: 1 - 19:27: 1

ch1	ch2	ch3	ch4	ch5	ch6	ch7	ch8	ch9	ch10	ch11	ch12	ch13	ch14	ch15
0	0	0	0	0	0	0	0	0	0	0	0	0	0	0

** m/s	dd deg	Tw deg C	Td deg C	humidity
9.0	229	5.5	5.4	100.00%

Record nos. 2935 - 2949
19:27: 2 - 19:48: 2

ch1	ch2	ch3	ch4	ch5	ch6	ch7	ch8	ch9	ch10	ch11	ch12	ch13	ch14	ch15
0	0	0	0	0	0	0	0	0	0	0	0	0	0	0

** m/s	dd deg	Tw deg C	Td deg C	humidity
9.7	231	5.6	5.5	100.00%

Grachical Representation Of The Data Of 19th And 20th 1858

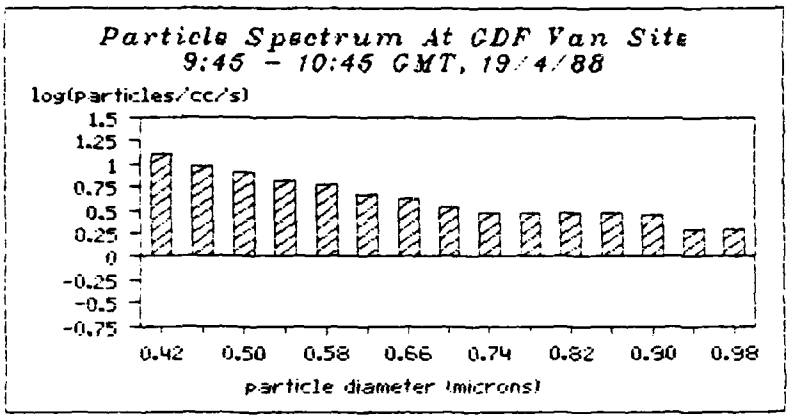
Particle Spectrum At CDF Van Site
9:45 - 10:45 GMT, 19/4/88
log(particles/cc/s)
1.5
1.25
1
0.75
0.5
0.25
0
-0.25
-0.5
-0.75
0.42
0.50
0.58
0.66
0.74
0.82
0.90
0.98
particle diameter (microns)

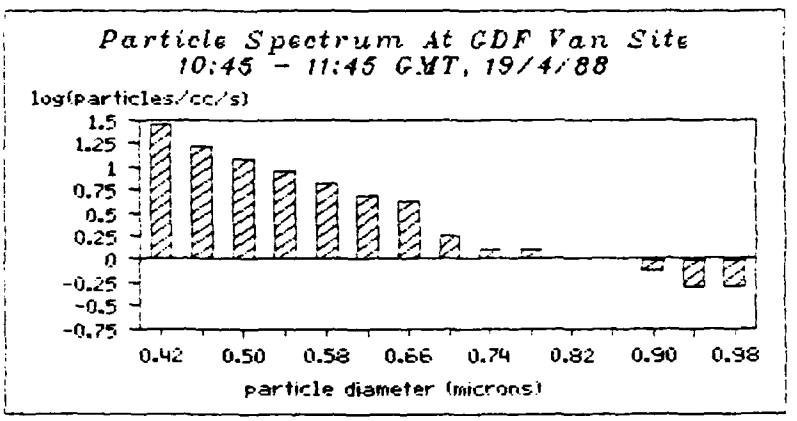
Particle Spectrum At CDF Van Site
10:45 - 11:45 GMT, 19/4/88
log(particles/cc/s)
1.5
1.25
1
0.75
0.5
0.25
0
-0.25
-0.5
-0.75
0.42
0.50
0.58
0.66
0.74
0.82
0.90
0.98
particle diameter (microns)

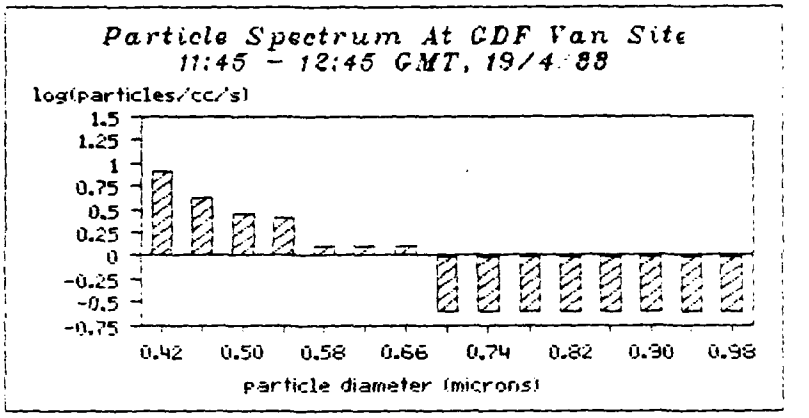
Particle Spectrum At CDF Van Site
11:45 - 12:45 GMT, 19/4/88
log(particles/cc/s)
1.5
1.25
1
0.75
0.5
0.25
0
-0.25
-0.5
-0.75
0.42
0.50
0.58
0.66
0.74
0.82
0.90
0.98
particle diameter (microns)

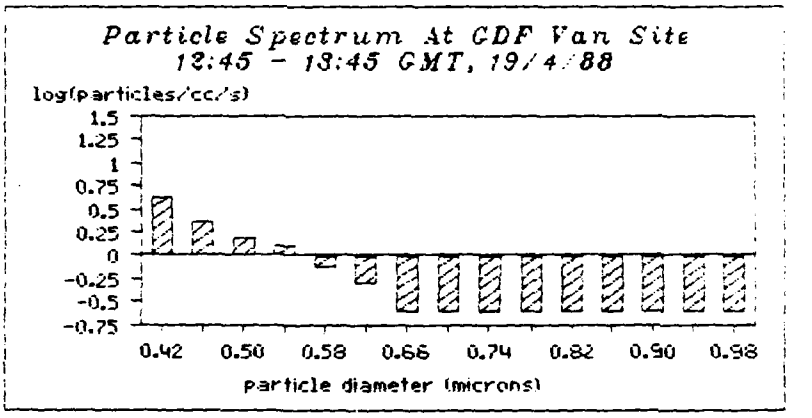
Particle Spectrum At CDF Van Site
12:45 - 13:45 GMT, 19/4/88
log(particles/cc/s)
1.5
1.25
1
0.75
0.5
0.25
0
-0.25
-0.5
-0.75
0.42
0.50
0.58
0.66
0.74
0.82
0.90
0.98
particle diameter (microns)

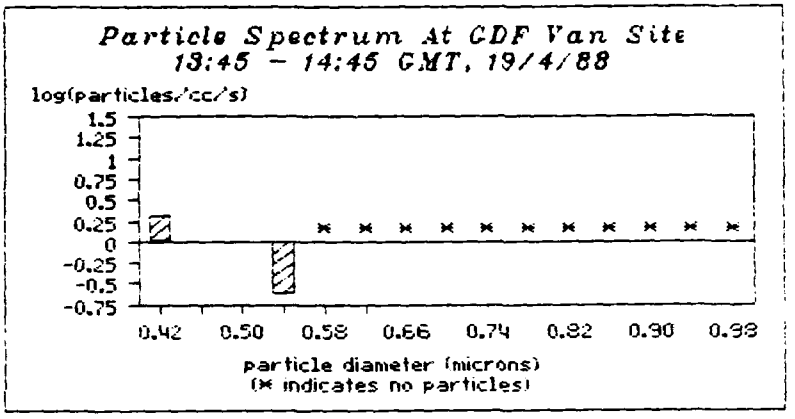
Particle Spectrum At CDF Van Site
13:45 - 14:45 GMT, 19/4/88
log(particles/cc/s)
1.5
1.25
1
0.75
0.5
0.25
0
-0.25
-0.5
-0.75
0.42
0.50
0.58
0.66
0.74
0.82
0.90
0.98
particle diameter (microns)
(× indicates no particles)

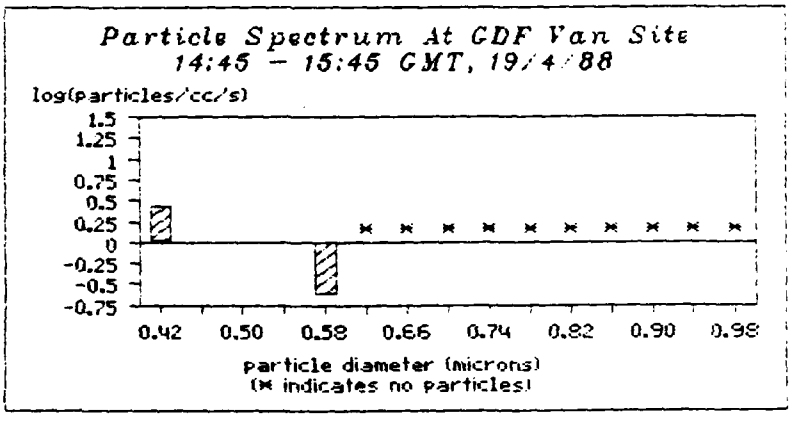
Particle Spectrum At CDF Van Site
14:45 - 15:45 GMT, 19/4/88
log(particles/cc/s)
1.5
1.25
1
0.75
0.5
0.25
0
-0.25
-0.5
-0.75
0.42
0.50
0.58
0.66
0.74
0.82
0.90
0.98
particle diameter (microns)
(× indicates no particles)

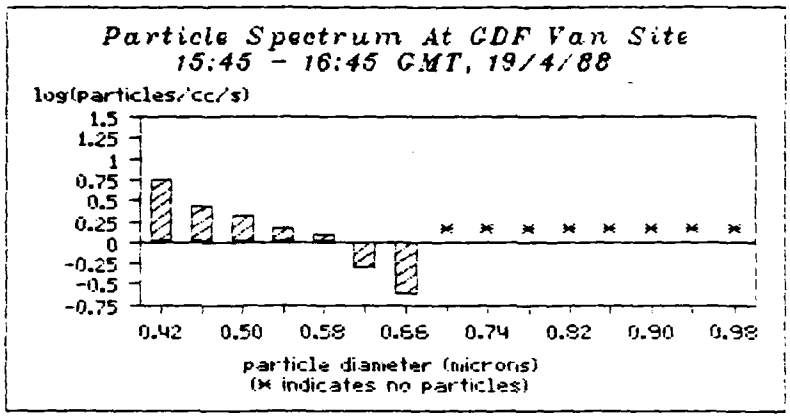
Particle Spectrum At CDF Van Site
15:45 - 16:45 GMT, 19/4/88
log(particles/cc/s)
1.5
1.25
1
0.75
0.5
0.25
0
-0.25
-0.5
-0.75
0.42
0.50
0.58
0.66
0.74
0.82
0.90
0.98
particle diameter (microns)
(* indicates no particles)

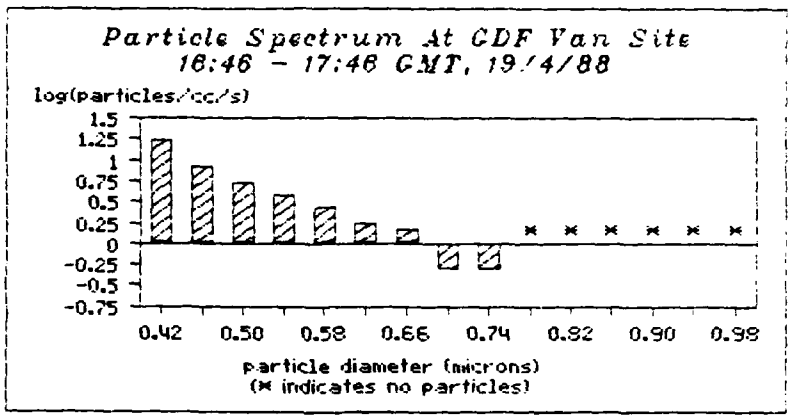
Particle Spectrum At CDF Van Site
16:46 - 17:46 GMT, 19/4/88
log(particles/cc/s)
1.5
1.25
1
0.75
0.5
0.25
0
-0.25
-0.5
-0.75
0.42
0.50
0.58
0.66
0.74
0.82
0.90
0.98
particle diameter (microns)
(* indicates no particles)

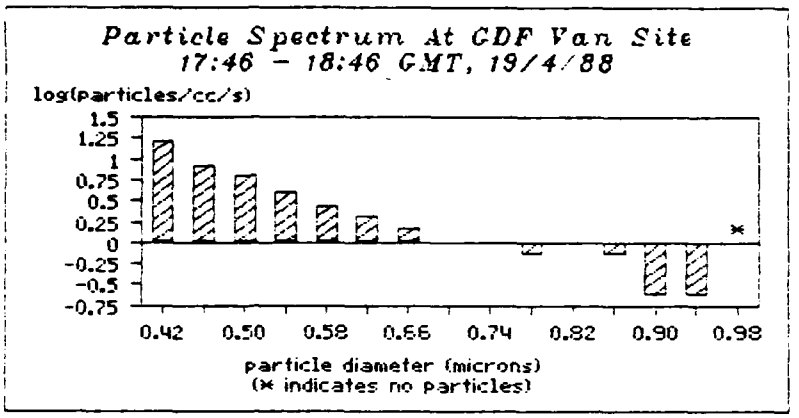
Particle Spectrum At CDF Van Site
17:46 - 18:46 GMT, 19/4/88
log(particles/cc/s)
1.5
1.25
1
0.75
0.5
0.25
0
-0.25
-0.5
-0.75
0.42
0.50
0.58
0.66
0.74
0.82
0.90
0.98
particle diameter (microns)
(* indicates no particles)

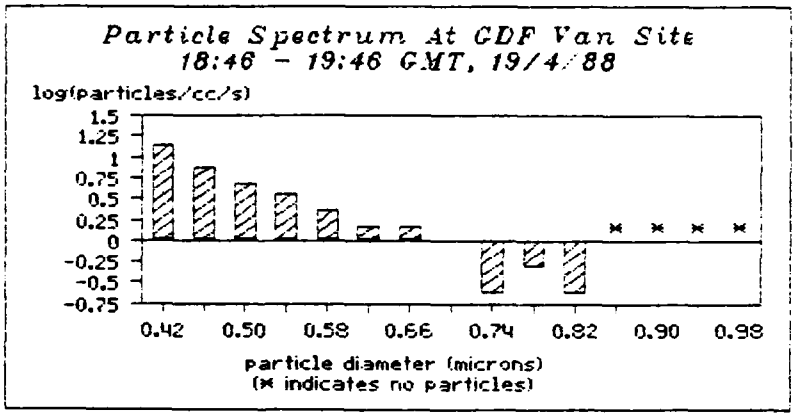
Particle Spectrum At CDF Van Site
18:46 - 19:46 GMT, 19/4/88
log(particles/cc/s)
1.5
1.25
1
0.75
0.5
0.25
0
-0.25
-0.5
-0.75
0.42
0.50
0.58
0.66
0.74
0.82
0.90
0.98
particle diameter (microns)
(* indicates no particles)

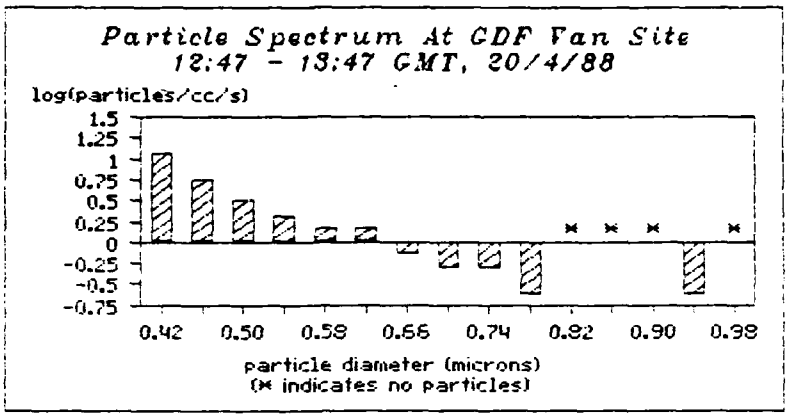
Particle Spectrum At CDF Van Site
12:47 - 13:47 GMT, 20/4/88
log(particles/cc/s)
1.5
1.25
1
0.75
0.5
0.25
0
-0.25
-0.5
-0.75
0.42
0.50
0.58
0.66
0.74
0.82
0.90
0.98
particle diameter (microns)
(* indicates no particles)

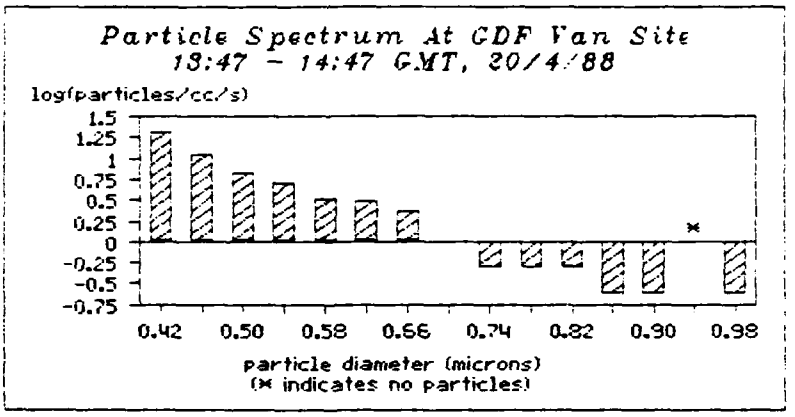
Particle Spectrum At CDF Van Site
13:47 - 14:47 GMT, 20/4/88
log(particles/cc/s)
1.5
1.25
1
0.75
0.5
0.25
0
-0.25
-0.5
-0.75
0.42
0.50
0.58
0.66
0.74
0.82
0.90
0.98
particle diameter (microns)
(* indicates no particles)

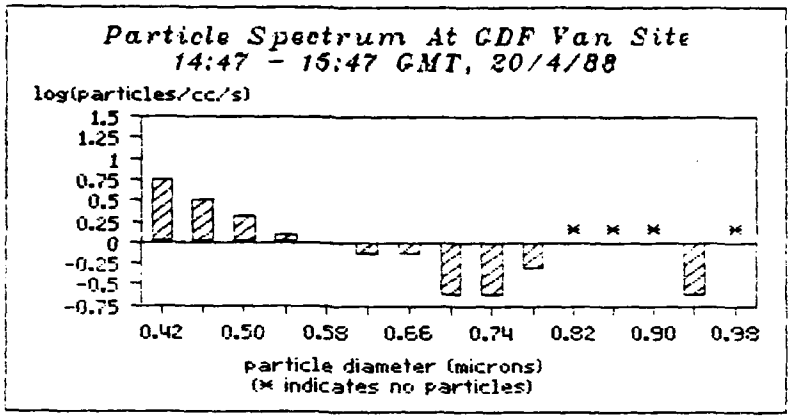
Particle Spectrum At CDF Van Site
14:47 - 15:47 GMT, 20/4/88
log(particles/cc/s)
1.5
1.25
1
0.75
0.5
0.25
0
-0.25
-0.5
-0.75
0.42
0.50
0.58
0.66
0.74
0.82
0.90
0.98
particle diameter (microns)
(× indicates no particles)

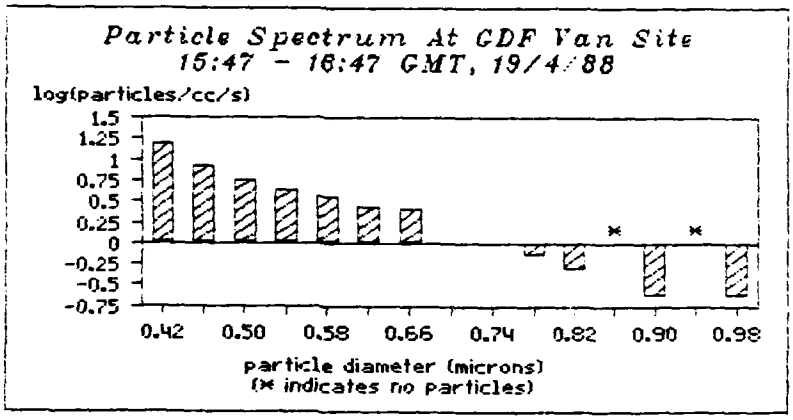
Particle Spectrum At CDF Van Site
15:47 - 16:47 GMT, 19/4/88
log(particles/cc/s)
1.5
1.25
1
0.75
0.5
0.25
0
-0.25
-0.5
-0.75
0.42
0.50
0.58
0.66
0.74
0.82
0.90
0.98
particle diameter (microns)
(× indicates no particles)

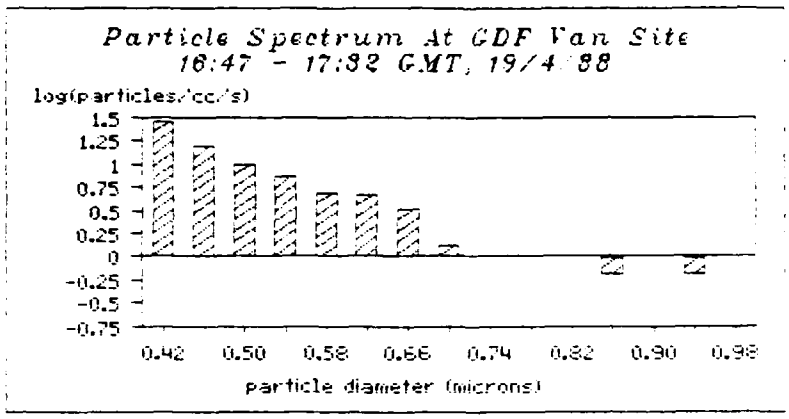
Particle Spectrum At GDF Van Site
16:47 - 17:32 G.MT, 19/4/88
log(particles/cc/s)
1.5
1.25
1
0.75
0.5
0.25
0
-0.25
-0.5
-0.75
0.42
0.50
0.58
0.66
0.74
0.82
0.90
0.98
particle diameter (microns)

Trajectory Analysis For 19th and 20th April 1988

19th April 1988

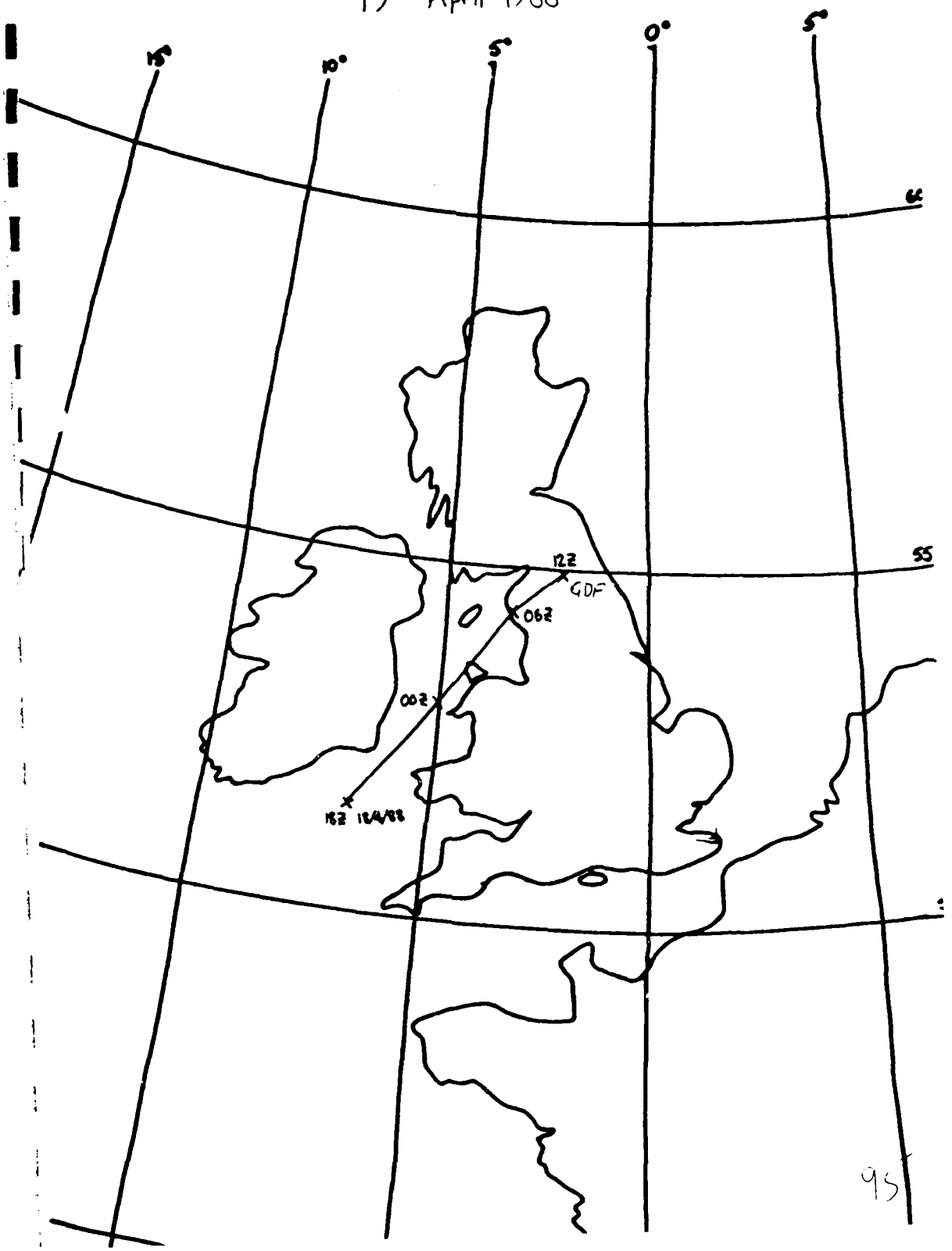

20th April 1988

SECTION 6

CONCLUSIONS

Measurements have been made of the deposition rate of aerosol to the surface by the occult, dry and rain-out processes. It has been demonstrated that the deposition rates of chemical agents when dissolved in cloud droplets are large, the deposition velocity being close to that for momentum to the same surface when the cloud is in contact with the ground. These values are at least 10x greater than the dry deposition velocity of natural aerosol to the same surface. This result suggests that a considerable enhancement of the deposition rates of soluble chemical agents is to be expected in elevated regions with complex terrain. The work has also shown that the effeciency of the rain-out process is substantially increased over elevated topography where the chemical agents are dissolved in the low level hill cap clouds. This process will give deposition rates of the chemical species 10x higher than the occult deposition rates although over the limited periods during which rainfall is actually occurring.